Fluorescence spectroscopy of single CdSe nanocrystals

By

John M. Lupton[1], Josef Müller[2]

[1]Department of Physics, University of Utah, Salt Lake City, Utah, USA
[2]Photonics and Optoelectronics Group, Physics Department and Center for NanoScience (CeNS), Ludwig-Maximilians-Universität München, Munich, Germany

1. Introduction

The true beauty of nature reveals itself in the delicate balance between order and disorder, between large and small scales. The leaves on a tree may appear to us as highly disordered at first glance, certainly once they have fallen to the ground; but their making relies on a high degree of order, a subtle interplay between physical processes and photochemical reactions in the light-harvesting complexes responsible for photosynthesis [1–3]. Indeed, this very process of photosynthesis has long caught the attention of researchers. Light from the sun is absorbed by pigments within such a complex, passed from molecule to molecule arranged in a particular order imposed by a protein scaffold, and funnelled to a sequence of reaction centres in which charge carrier separation, protonation, and ultimately the formation of glucose take place. At first sight these complexes appear suitably rigid and ordered [4]. Yet detailed theoretical investigations [2] along with high-resolution spectroscopy in the time [3] and frequency domain (i.e. single molecule spectroscopy) [5, 6] have revealed that a high degree of order – the spatial arrangement of pigments – is not the only horse nature places its bet on.

Consider the simplest case of fluorescence energy transfer from one molecule to another, a straightforward dipole–dipole coupling problem. As in antenna theory, the maximum coupling efficiency occurs if both the transmitter and receiver are in resonance. In a molecular picture, this translates into a spectral overlap between absorption and emission of donor and acceptor. If the individual pigments experience a high degree of local order, their optical transitions will be extremely narrow. However, some change in transition energies is inevitable from molecule to molecule due to miniscule differences in the local environment, isotopic effects, isomeric effects, and the likes [7]. The net result is that dipolar coupling breaks down, and excitation energy becomes localised [8]. This effect is akin to disorder localisation, well-known from transport theory. As in multiple trapping transport theory, however, dynamic disorder can help overcome the effect of static disorder. Temporal fluctuations in the local electronic structure of the individual molecular entity can actually promote microscopic fluorescence resonance energy transfer (FRET) [2]. In

a light-harvesting complex, the protein scaffold ensures that all pigments are situated in the correct geometry, optimized by evolution. On the other hand, proteins are dielectrically dynamic objects, imposing a rapidly varying dielectric environment on the local pigments. Consequently, the effective electronic transitions broaden [6], improving FRET between adjacent pigments [2, 3].

The temporal fluctuations of nanoscale emitters and absorbers – spectral diffusion – constitutes the central theme of this chapter. Semiconductor nanocrystals are excellent systems to investigate random fluctuations in the emission properties of a light source in the single photon limit [9, 10]. Along with the intensively studied fluorescence intermittency [11–26] – fluorescence blinking – the seemingly random spectral fluctuations follow a well-defined pattern which can provide insight into either the immediate dielectric environment and nature of the emitting species or the overall nanoparticle shape [27, 28]. Indeed, suitable choice of the immediate surrounding of the semiconductor surface can even virtually suppress blinking [29, 30]. As nanocrystals are significantly larger than most dye molecules studied in single molecule investigations [31], spectral fluctuations correspond to changes in the properties of the primary excitonic species. These properties are controlled by surface states of the nanocrystal, which can acquire a net charge [32–35], in turn polarising the exciton. Whereas most blinking studies have been carried out at room temperature in the past, the most profound insight into these subtle fluctuations is available at cryogenic temperatures, where the elementary transitions become orders of magnitude narrower than the ensemble spectrum [36].

This chapter serves to review some of the recent progress made in studying and exploiting the spectral characteristics of individual CdSe nanocrystals. After discussing some of the basic experimental techniques, the spectral fluctuations of a particularly interesting class of CdSe nanocrystals are highlighted. Building on the seminal demonstration of shape control in inorganic semiconductor nanoparticles [37], these CdSe spherical quantum dots are surrounded by an elongated CdS shell and support, in contrast to purely spherical particles, linearly polarised emission [38]. The broken symmetry of the system results in spatial separation of the electron and hole wave functions, which can be controlled by external electric fields. Such fields are created by surface charges, which in turn control the optical properties such as the transition energy, transition line width, intensity, and electron–phonon coupling strength of the single emitter. The spectral jitter observed follows a well-defined pattern and exhibits either Gaussian or Lorenzian statistics. It is illuminating to draw parallels to seemingly unrelated classes of nanoscale light sources, conjugated polymers. Although the electronic properties of these carbon-based systems are very different, near identical spectral fluctuations are observed, which indicate the role of highly local dielectric effects. Finally, an example is presented on how to put the spectral properties of single, highly polarisable nanoscale light sources to work. Electric fields enable a tuning of the excitonic transition so that the dipole–dipole coupling strength in a microscopic, single particle FRET couple can be controlled. This electrical control of energy transfer constitutes a nanophotonic field-effect switch, or FRET gate, which, with suitable self assembly techniques, may well provide a building block for future nanophotonic circuitry. Most importantly, however, this electrical tuning of the elementary transition opens a window to

control order effects in nominally disordered systems, by driving a microscopic transition in and out of resonance.

2. Why single particle spectroscopy?

Every nanocrystal is different. Sizes vary from particle to particle, shapes differ ever so slightly, and even the atomic composition, the isotopic distribution, becomes significant for extremely small particles. Most importantly, every particle experiences a slightly different dielectric environment. CdSe nanocrystals are stabilised internally through ionic bonds. However, the smaller the particle becomes, the greater the percentage of atoms forming the crystal sitting at the surface. These surface atoms are characterised by only partially saturated bonds and can therefore form dangling bonds. Many of these surface states are pacified sufficiently by organic ligands, which also serve to stabilise the nanocrystals in solution and prevent aggregation and precipitation [39]. The crucial influence of these ligands on the optical properties is well documented: removal of the ligands by, e.g. exposure of the particles to the electron beam of a transmission electron microscope results in non-emissive particles in which the fluorescence is quenched [40]. However, these ligands form a thermodynamic equilibrium with the particles in solution, continuously binding and unbinding, which necessitates a surplus of ligands. A simple experiment reveals this effect. When compared to organic dye molecules, nanocrystals are reasonably stable to environmental influences such as oxidation. However, the temporal stability of the fluorescence of a solution of nanocrystals depends on concentration. The stability of the emission intensity under constant illumination in part depends on the process of statistical aging, which constitutes the ensemble average of single particle blinking [41–43]. As this phenomenon follows a scale-invariant power-law distribution of the probabilities of detecting a particular duration over which the emission of the particle remains "on" or "off" under constant excitation [44], the probability for increased "off" periods increases within an ensemble of nanocrystals with time. In the absence of illumination, serial dilution of a nanocrystal solution by addition of pure solvent reduces the ratio of free ligands to particles, thereby ultimately lowering the overall surface coverage. The effective result is that nanocrystals can degrade in highly dilute solutions, a phenomenon which can be counterbalanced through the addition of further ligands.

In any case, both the charged surface of the nanocrystal and the surrounding ligand shell constitute a variable nanoscale dielectric environment, which can influence the elementary electronic transition and therefore lead to a difference in transition energy from one nanocrystal to the next. This distribution of transition energies between particles within the ensemble is referred to as inhomogeneous broadening [45]. Each particle, however, has its own intrinsic spectral width. The quantum mechanical limitation of spectral width Γ is given by the Heisenberg uncertainty principle through the radiative transition time τ, $\Gamma \geq h/4\pi\tau$. This relation between transition line width and transition time only applies in the limit of coherence loss through population loss, i.e. through an electronic transition. There are other conceivable routes to reducing the electronic coherence time – that is, the time, in which the excited electron wave function retains its phase – in an individual

emitter, such as through electron–phonon scattering or any other form of nuclear motion. This homogeneous line width, controlled only by the loss of coherence in the excited state, constitutes the primary limitation to the spectral width of the emission and absorption of a single particle [46]. Long-phase coherence is particularly interesting for demonstrating quantum mechanical coupling between quantum dots, a prerequisite for optical quantum computing [47]. However, random fluctuations in time of the local dielectric environment of the particle provide a further form of inhomogeneous spectral broadening, spectral diffusion. Single particle measurements can therefore, in principle, offer access to the energetic *limitations* of homogeneous broadening [48]. Time-dependent studies of the single particle emission open a window to some of the spectral broadening processes.

3. Experimental approach

There are two principal routes to study the emission of a single quantum dot: either the optical collection volume is minimized, e.g. through the use of suitable spatial apertures imposed either on the emitters [49, 50] or on the detector as in the case of near-field scanning microscopy; or by reducing the number of emitters present in the far-field optical collection volume. The latter is rather facile to achieve in solution-based quantum dots (but not so in vapour phase, epitaxially grown nanostructures) by simple serial dilution, keeping in mind the limitations with regards to stability of the ligands mentioned above. As the spatial resolution of an optical microscope is roughly limited to the dimensions of the wavelength of light involved, spacing particles further than $\sim$500 nm apart should allow optical spectroscopy to differentiate between the electronic properties of individual particles. Ideally, the particles are fixed in space, as particles in dilute solutions would drift in and out of the microscope focus. Fortunately, most particles are readily dispersed in common polar (e.g. poly(vinyl-alcohol)) or non-polar (e.g. polystyrene, poly(methyl-methacrylate), Zeonex) matrices, which can be spin-coated on quartz glass substrates to yield highly uniform films of optical quality, tens to hundreds of nanometers thick. These films are then studied using either a confocal scanning or a wide-field imaging microscope [24]. The experiments reported in the following were all carried out using a wide-field setup, which offers the key advantage of being able to record multiple emitters (i.e. microscope fluorescence spots) simultaneously [51]. In brief, the microscope used employed a long working distance (8 mm) microscope objective lens with a (comparatively small) numerical aperture of 0.55. This lens allowed the collection of light emitted by a nanoparticle film mounted in a cold-finger helium cryostat under vacuum. The nanoparticles were excited by an argon ion laser (typically at 488 nm), focused to a spot of approximately 100 μm in diameter incident at a non-vertical angle on the substrate. The fluorescence, collected by the microscope objective lens, was spectrally dispersed in a monochromator and recorded by a CCD camera of appropriate sensitivity.

Figure 1 illustrates the key properties and strengths of the experimental setup. Figure 1a shows the CCD image of a substrate covered with a highly dilute nanocrystal–polystyrene dispersion. The entrance slit of the detector was closed in horizontal direction such that in the collection plane along the y-axis typically only

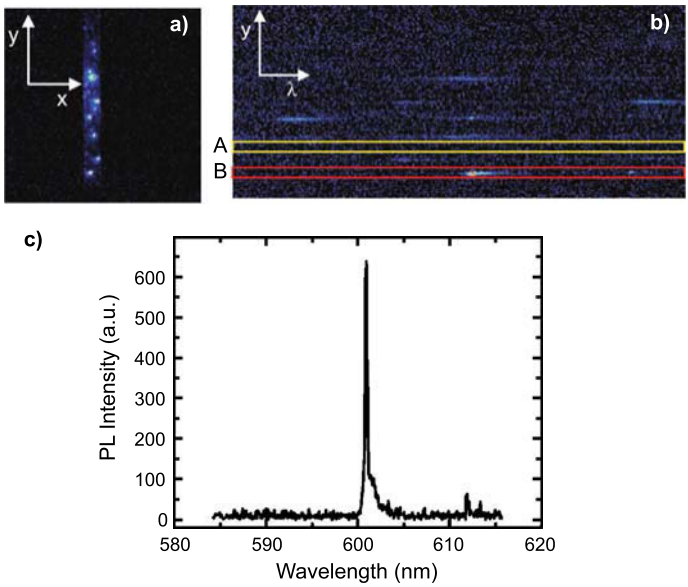

Fig. 1. Single particle detection and spectroscopy. **a** The spatial region of the microscope image projected onto the CCD camera is defined by a horizontal entrance slit so that only one single particle (seen as a bright spot) is visible in the horizontal direction. The image corresponds to a region of approximately 60 µm height on the substrate. The fluorescence light is subsequently passed through a monochromator and spectrally dispersed so that the *x*-component of the image now corresponds to wavelength λ **b**. The spatial information of the location of the particles is maintained in the *y*-direction. The regions A and B mark the background fluorescence and a typical single particle emission spectrum, respectively. **c** shows a typical single particle photoluminescence spectrum at 5 K. Adapted from [51]

one nanocrystal is detected at once, manifested by a fluorescence spot on the CCD camera. The typical spacing between single nanocrystals is 5–10 µm. In order to carry out spectroscopy on the single particle, the emitted light is dispersed spectrally in a grating spectrometer. Figure 1b shows exactly the same spatial image as recorded in (a), but now resolved by emission wavelength. Consequently, the *x*-axis of the emission now corresponds to the wavelength of emission, whereas the spatial information in *y*-direction is maintained. The emission intensity is encoded in the colour of the image. The image illustrates the role of the entrance slit in spectroscopy: if more than one particle is present in the *x*-direction of the image in (a), multiple fluorescence peaks or spectral broadening would be observed in (b). As a large area is excited by the impinging laser light, the imaging technique offers a facile way to correct for any residual background emanating from the matrix or the substrate. Choosing a region of interest (A) immediately besides the nanocrystal image (B) in Fig. 1b defines the fluorescence background, which can subsequently simply be subtracted from the emission spectrum. Figure 1c illustrates a typical example of a single particle fluorescence spectrum, recorded for a CdSe/CdS nanodot/nanorod at 5 K: a narrow transition is observed around 602 nm, which is somewhat broadened to longer wavelengths.

As one expects, this emission spectrum of the single particle at low temperatures is substantially narrower than the bulk emission. Figure 2a illustrates an ensemble

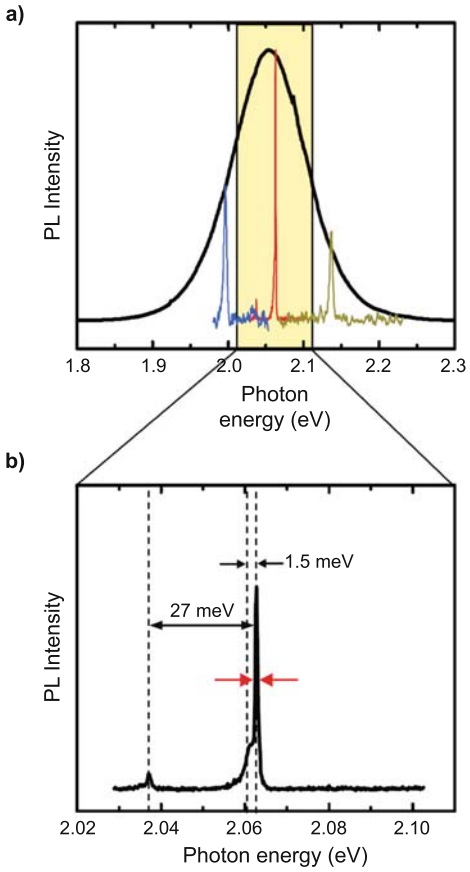

Fig. 2. Comparison of single particle line width to the inhomogeneous broadening of the ensemble. **a** Three characteristic single particle spectra, recorded at 5 K, superimposed on the ensemble fluorescence spectrum. **b** A typical low temperature fluorescence spectrum, showing a narrow zero-phonon line, an acoustic phonon side band, and an optical phonon progression. Adapted from [51]

emission spectrum at room temperature with three characteristic single particle spectra superimposed. The bulk emission spectrum constitutes the sum over many single particle spectra, recorded from different spots seen in the CCD image. The width of the ensemble spectrum is primarily defined by the energetic scatter from one particle to the next. Figure 2b displays a close-up of one of the emission spectra. The transition line width in this case is 800 μeV, over 130 times narrower than the ensemble spectrum. A hump is visible on the low energy side of the spectrum, characteristically offset by roughly 1–2 meV. This hump, which is well-known from spectral hole burning measurements [52], an alternative way of determining the elementary transition width of a particular energetic subset of the ensemble, corresponds to the acoustic phonon side band, or phonon wing. Interestingly, due to the finite size of the semiconductor nanocrystal, the acoustic phonon modes become quantized [53] rather than forming the continuum of states familiar from the

Debye approximation of heat capacities in solid state physics. The discrete acoustic phonons, a collective breathing motion of all of the atoms constituting the crystal, are typically observed around 1 meV and simply depend on the size of the crystal. Significantly offset from the narrow peak by approximately 27 meV is a further emissive feature, which corresponds to the optical phonon side band of the emission. This optical phonon is characteristic of the CdSe ionic bond, and immediately reveals that recombination, and thus electron–phonon coupling, occurs in the CdSe part of a CdSe/CdS core/shell nanocrystal. To a first approximation, the narrow transition can be referred to as a zero-phonon line, as it is purely electronic in nature. As will be discussed in the following, the line, which is still two orders of magnitude broader than spectra reported using the technique of resonant spectral hole burning [54], is significantly broadened by spectral diffusion. In contrast to spectral hole burning, however, single particle measurements immediately provide us with information relating both to the random scatter from particle to particle, as well as the intrinsic electronic properties and dynamics. Most importantly, spectroscopy on a single particle can enable us to relate far-field spectral information to the nanoscale physical properties of the particle such as its shape. As spectral hole burning probes a homogeneous subset of an inhomogeneous ensemble, shape effects are generally masked in amorphous systems through random orientations. It is also worth noting that fluorescence excitation spectroscopy is a further interesting technique to study the electronic structure of single nanocrystals [55]. Although all of the initial single molecule fluorescence experiments were carried out in excitation using a narrow-band, tuneable laser [7], nanocrystals are usually studied non-resonantly as the broad absorption spectrum of nanocrystals arising from a continuum of states makes it possible to observe the fluorescence from the relaxed state of lower energy. Remarkably, excitonic features can be discerned within the continuum of states of a single particle, providing insight into higher lying states [55].

4. Spectral dynamics of single nanocrystal emitters: signatures of particle shape

The following discussion will focus on a particularly interesting class of CdSe/CdS nanocrystals, in which a spherical CdSe core is capped on one end by an elongated CdS rod-like structure [38]. The transmission electron microscope image in Fig. 3 displays a typical structure of a single particle. The high degree of crystallinity of the nanoparticle is visible through the diffraction planes in the microscope image. One end of the particle is somewhat more bulky than the other and corresponds to the CdSe nucleus, with a slightly smaller band gap than the CdS structure growing out of one side on the $\{0\,0\,\bar{1}\}$ facet of the CdS nanocrystal. The typical aspect ratio of these particles is 1:4, with lengths ranging between 15 and 20 nm. These nanocrystals of mixed dimensionality are particularly interesting for single particle experiments – and, as will be discussed later on, for FRET studies – as the absorption cross section of a particle increases with physical size. Because of the electronic structure of the particle – the CdS band gap is larger than the CdSe gap, forming a type I heterostructure – emission always occurs from the CdSe unit, as witnessed by the CdSe optical phonon seen in the single particle spectra. The

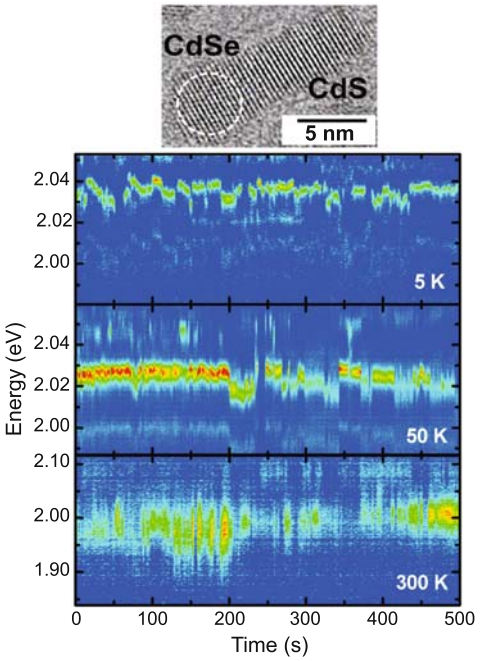

Fig. 3. Spectral diffusion in the fluorescence of single elongated CdSe/CdS nanocrystals at 5, 50 and 300 K. The photoluminescence spectra are plotted as a function of time in a two-dimensional representation with the intensity encoded in colour scale (blue: low intensity, red: high intensity). The temporal resolution of the data is 1 s. The transmission electron microscope image of a single nanocrystal is shown, with the CdSe core region indicated by a white circle. Adapted from [27]

absorption can therefore be enhanced without fundamentally changing the emission properties. Figure 3 illustrates three typical single particle fluorescence time traces, recorded in 1 s integration windows. The *x*-axis of the plots corresponds to time, whereas the *y*-axis indicates the energy of the emitted photon. Dark blue marks low emission intensity, and yellow-red indicates high intensity. The two-dimensional representation therefore displays the time evolution of the emission spectra. Three different temperatures are shown, which primarily control the spectral width and the temporal stability of the transition.

At first sight, the spectra appear to be rather similar for the different temperatures. However, as the temperature is raised from 50 to 300 K, the spectra broaden 30-fold and appear to exhibit more rapid fluctuations. The spectral time traces display both spectral jitter, which is the focus of the present discussion, and fluorescence intermittency, in which the emission suddenly vanishes and the intensity, marked by the colour code in the two-dimensional plot, returns to the background level. Whereas spectral transitions appear more continuous at room temperature, the low temperature traces suggest both continuous jitter and sudden, larger, spectral jumps [56]. Qualitative inspection of these time traces is limited, but as discussed in the following, there are a few facile analyses which can be applied to reveal a plethora of phenomena and correlations.

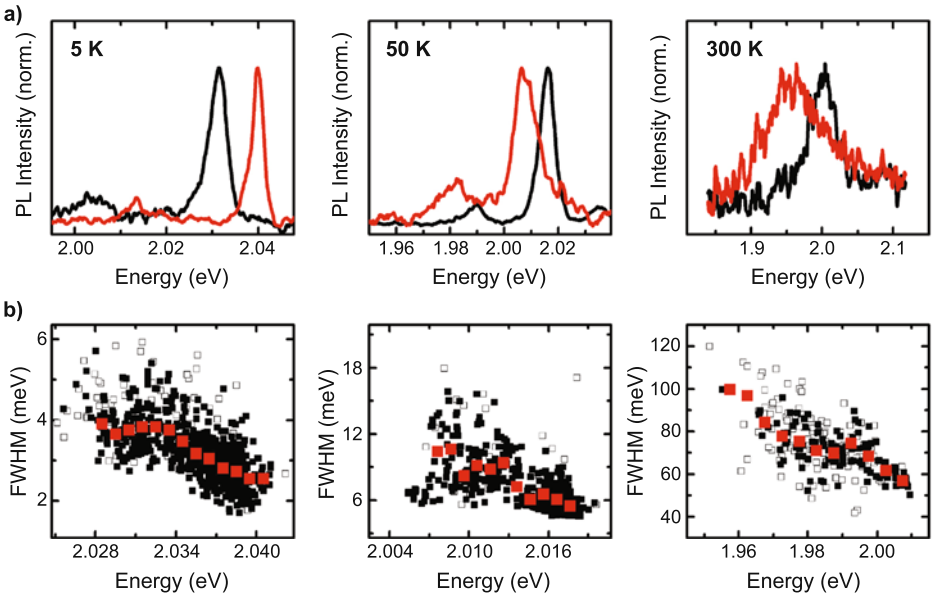

Fig. 4. Correlation between peak position and peak line width for three different particles recorded at 5, 50 and 300 K. **a** Two representative spectra taken from the traces in Fig. 3, illustrating a spectral broadening concomitant with the spectral red shift. **b** Correlation between spectral line width and peak position. Adapted from [27]

The first piece of information which can be derived from the spectral traces is the fluorescence peak energy and the spectral line width. Figure 4a displays two example spectra extracted at each temperature. As is particularly visible at room temperature, the lower energy spectra appear to correlate with a broader emission band. Figure 4b provides a more systematic analysis of the traces shown in Fig. 3 by plotting the spectral line width against the spectral peak position for each of the spectra comprising Fig. 3. The correlation in the data is unambiguous: as the emission shifts to the red, the spectrum broadens. The open symbols indicate the raw data, which clearly display significant scatter. The scatter can be reduced by limiting the consideration to data points (solid squares) for which only spectral shifts were considered which occurred on time scales longer than the measurement window of 1 s. The correlation can be further highlighted by displaying a binned average, as indicated by the solid squares in the figure.

Much of scientific methodology revolves around the identification of correlations, so a clear correlation between spectral line width and transition energy of the single particle must carry a physical meaning. It was soon realised in the spectroscopy of single nanocrystals [57–59], and indeed of single epitaxially grown quantum dots [60–62] and molecules in general [63], that the spectral properties of the individual emitter can be modified by fluctuations in the local dielectric environment. Nanocrystals carry their own local dielectric environment in the form of organic ligands and a large density of surface defects. Empedocles and Bawendi were able to relate the spectral shifts observed in single particle fluorescence as a function of time to

electric field effects, by studying the influence of external electric fields on the emission properties at low temperatures [64]. Local charges on the surface of the nanocrystal result in an effective electric field [65, 66] which the exciton within the nanocrystal experiences. The charges therefore provide an additional potential which controls the electron-hole wave function overlap, and therefore the transition energy [62]. Core-shell nanocrystals are prototypical materials to study the quantum-confined Stark effect [67], in which the exciton gains a high degree of polarisability due to the ability to push one wave function into the core and the other into the shell under application of a field. To a first approximation, there are two principal routes by which local charges, accumulated on the surface of the nanocrystal, can influence the emission [64]. The appearance or disappearance of a surface charge will result in a sudden jump of the transition energy. On the other hand, once surface charge has been formed on the nanocrystal, it may redistribute with time, leading to a slight variation in distance to the exciton. Consequently, the exciton experiences a temporally varying electric field and thus displays a change in transition energy with time. If this change in transition energy occurs on time scales shorter than the measurement window (in the present discussion, typically 1 s), the spectral shift of the transition will manifest itself as a spectral broadening. In a perfectly symmetric particle, changes in the mean position of the surface charge should not influence the transition energy, but only changes in the surface charge density. Consequently, in a perfectly spherical nanocrystal there should not be a correlation between transition line width and peak energy, as remarked by Empedocles and Bawendi [64]. Most particles are, however, not perfectly spherical – least of all the CdSe/CdS hetero-structure nanorods. Interestingly, similar spectral correlations were recently reported for much larger CdS nanorods which are outside of the regime of quantum confinement [68]. This observation suggests that emission in these large rods occurs from localised regions, which can then in turn become sensitive in their emission to surface charges.

Figure 5 illustrates a possible scenario for the physical origin of the correlation of line width with transition energy. Figure 5b summarises the electronic structure of the nanocrystals. The offset between conduction bands of the CdSe and the CdS is minimal so that the electron can delocalise from the CdSe core into the CdS shell. The CdSe valence band is, however, significantly lower in energy so that the hole of the exciton becomes localised in the CdSe – hence the CdSe optical phonon in the single particle emission. As a potential is applied to the particle ($F > 0$), the electron wave function can delocalise further into the CdS shell as the external potential screens the internal Coulombic attraction between electron and hole. This reduces the confinement energy of the electron–hole pair, leading to a red shift in the emission. Surface charges, as indicated in the cartoon in Fig. 5a, lead to the formation of an effective potential and thus to local electric fields. As the exciton is localised to one end of the elongated nanocrystal, in the CdSe core, the spatial position of the surface charge along the shell determines the transition energy. On the right hand side of Fig. 5a, the surface charge is situated far from the core. Consequently, the emission appears at the higher end of the spectrum. As the surface charge moves around the surface of the nanocrystal randomly in the course of the spectral measurement, different effective quantum-confined Stark shifts are probed. The envelope of these

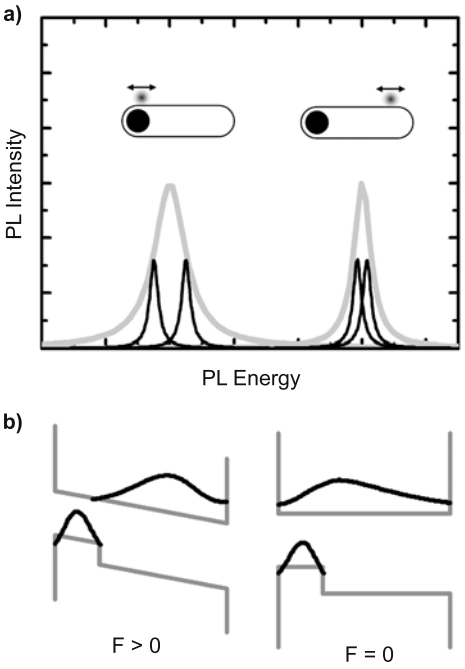

Fig. 5. Schematic representation of the influence of surface charge density on the emission from a single elongated nanocrystal. **a** Surface charge present at two different distances from the core of the nanocrystal, in which the hole of the exciton is localised, results in different magnitudes of a Stark shift in the emission. As the detection of the emission spectrum occurs over a finite time, spatial jitter in the charge density will result in spectral broadening. The closer the surface charge is located to the core of the nanocrystal, the stronger the red shift and the stronger the line broadening. **b** The electric field F induced by the surface charge also results in a perturbation of the electron–hole wave function overlap within the nanocrystal and thus of the radiative rate. A large local electric field leads to a displacement of the electron with respect to the hole and therefore reduces the wave function overlap and the radiative rate. Under the assumption of constant non-radiative decay, this change in wave function overlap results in a reduction in photoluminescence intensity. Adapted from [27]

different effective spectra seen within a particular temporal measurement window is indicated. This spectral envelop is significantly narrower if the surface charges are situated far from the CdSe core, assuming a random spatial fluctuation amplitude of the charges which is independent of the position on the nanoparticle surface. As the surface charges move closer to the core, the emission shifts to the red, but as the effective Stark shifts become larger, the overall envelope function broadens: the peak position correlates with the spectral width.

Although it was initially noted that such a correlation should not be observed in spherical nanocrystals [64], it was recently reported in room temperature spectroscopy [69]. However, as the transmission electron microscope images of [69] show, the term “spherical” is somewhat open to interpretation. From the cartoon in Fig. 5 it can be inferred that even the slightest breach in particle symmetry will lead to a correlation of line width with transition energy. The smaller the particle, the greater the sensitivity to a miniscule perturbation of shape. In addition, the internal field of

the ionic lattice [70] of the nanocrystal should also play a role, although this aspect has thus far only received little attention. Spectral fluctuations can be equally influenced by fluctuations in the equilibrium coordinates of the atoms constituting the ionic crystal. This phenomenon is primarily electrostatic – or electrostrictive – in nature, and could also lead to a correlation of line width with energy, but only under the premise of a breach in spherical symmetry. Such a breach is conceivable through an atomic defect [71].

A simple electrostatic model can qualitatively explain the correlation observed [72]. Figure 6 shows a plot of line width–peak position correlations for three different temperatures, with the data accumulated over five particles each comprising a total of approximately 7000 spectra. The peak shift was determined by subtracting the peak position of the bluest spectrum recorded for the particle. The spectral range of 30 ± 10 meV over which peak shifts occur is virtually independent of temperature, although the average line width of the spectrum increases by almost two orders of magnitude with increasing temperature. For all temperatures, the spectral width

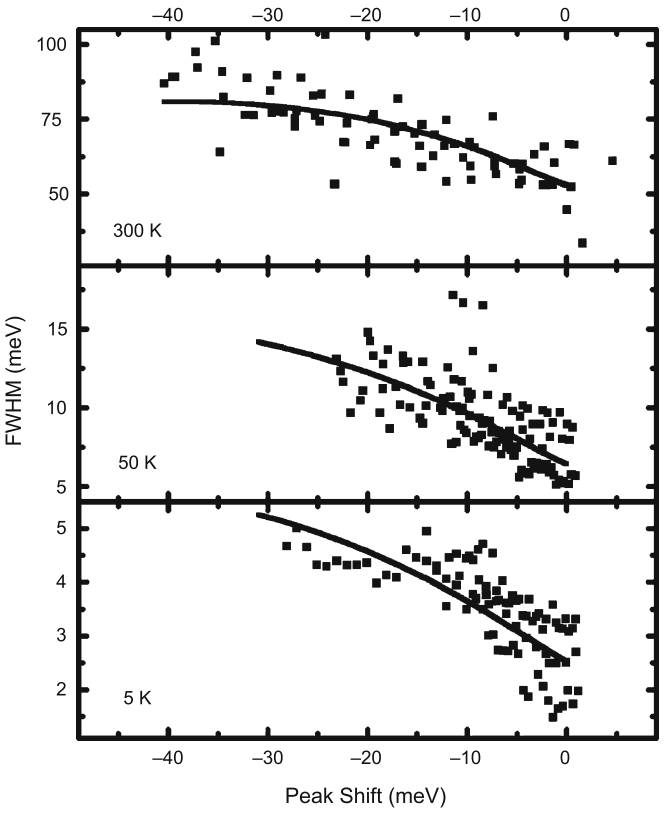

Fig. 6. Temperature dependence of line width–peak shift correlations. The data extracted for a total of five single nanocrystals are shown for each temperature. The solid line represents the quantum-confined Stark effect shift and resulting spectral broadening calculated for a single charge moving along the long axis of the nanocrystal. Adapted from [28]

varies by a factor of two during the spectral diffusion. The observation of correlated spectral diffusion at room temperature is somewhat surprising, yet fully consistent with the model proposed above. The spatial amplitude of surface charge oscillations, i.e. the average distance moved randomly by the charge distribution in a given time, should depend on temperature, but not the effect of the local field on the spectral position as induced by the quantum-confined Stark effect. The larger oscillations simply imply that the spectra broaden with increasing temperature. The maximum and minimum fields that surface charges can exert on the CdSe core, however, must be independent of temperature, and therefore the overall energy range over which drifts can occur during a measurement [28].

Although one can only speculate on the nature of the surface charges, the consistency of the phenomenological model can be verified by estimating the field effect of a single charge migrating along the long axis of the particle. Assuming a polarisability of the nanorods comparable to spherical NCs [64] and following the equations in [64, 72], a single charge must be separated from the core by about 3 nm to induce a Stark shift of 40 meV. This spatial separation is in good agreement with the diameter of the nanorods, as seen in the microscope image in Fig. 3. By moving the charge along the nanocrystal and considering a constant fluctuation in position one may estimate the dependence of line width on relative peak position, as shown by the solid lines in Fig. 6. As the quantum-confined Stark effect is minimal when the charge is situated at the far end of the nanorod (i.e. far from the core), yet a finite line width is measured, a line width offset has to be considered due to residual broadening at zero peak shift. Sources of this residual broadening may be charge fluctuations on time scales shorter than the measurement; or electronic dephasing induced by strong phonon scattering. The free fitting parameter in this simple model is the magnitude of spatial oscillations, which is determined as 0.2, 0.6 and 2.2 nm for 5, 50 and 300 K, respectively [28]. The 5 K value is of the order of the typical distance between ligands, respectively surface defects [73]. The simplest conceivable model of one-dimensional charge transfer along the nanorod thus provides both qualitative and quantitative agreement with the data. As it is the overall change in field which is of primary interest and not the actual charge distribution, the dynamics of the charge distribution can be well approximated by the dynamics of a single point charge. In addition, it is helpful to note that even if the spatial amplitude of charge oscillations were not constant along the rod, the experimental correlation would still provide a measure of charge *migration*, although this would complicate the microscopic model.

Evidently, the room temperature spectra are broader than the maximal achievable spectral shift due to the Stark effect of $\sim$40 meV. Even if the oscillations of surface charge were so strong that the charge were completely annihilated and created during the detection window of 1 s, it is unlikely that local field-induced oscillations account for the observed spectral widths of 100 meV. This implies a second contribution to line broadening at room temperature, which is due to efficient exciton scattering on optical phonons, representing a very rapid dephasing process [74]. Whereas the low temperature single nanocrystal lines are inhomogeneously broadened by spectral diffusion and do not provide insight into dephasing processes, the observed spectral diffusion dynamics suggest that the opposite is true for room temperature measurements. To a first approximation, one may conclude that the narrowest spectra at room

temperature (∼50 meV width) are predominantly homogeneously broadened due to the phonon scattering-induced ultrafast dephasing [28].

Although the correlation between transition energy and fluorescence line width is clearly discernible in a wide range of single particle experiments, the data points in the correlation plots scatter widely. This scatter results from the fact that the fluorescence traces also contain temporal information, besides the spectral information relevant to the correlation. If the proposed model of a surface charge-induced change in electron–hole wave function overlap is correct, a spectral shift should also go hand in hand with a change in the radiative rate and thus a change in emission intensity. In addition, the optical phonon seen in the single particle spectra at 27 meV to the red of the zero-phonon line should be influenced by a change in local electric field, as it results from the vibration of a the polar CdSe bond. The coupling strength of electrons to such Fröhlich phonons changes with electric field so that a red shift in the emission energy should result in an increase in phonon coupling strength in the emission [45]. Such more detailed correlations are not immediately apparent from the raw data traces. However, there is a straightforward means of improving the data quality by performing a manipulation akin to boxcar averaging to remove the redundant temporal information from the fluorescence trace. To do this, the spectra in the trace are sorted with respect to the peak position, thereby removing the time dimension [27]. Figure 7 shows a plot of the normalised raw data, simply sorted by emission peak energy (which is marked on the *x*-axis). Without performing any further manipulation, two important features are immediately obvious from this trace: as the peak energy shifts to lower energy, the spectra become broader, giving the two-dimensional representation a funnel-like appearance. In addition, the

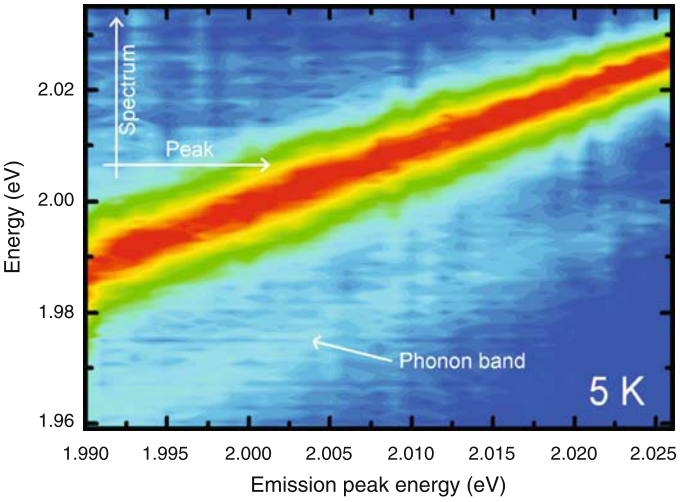

Fig. 7. Boxcar averaging of a single particle fluorescence trace to remove the temporal noise. The photoluminescence spectra of one single nanocrystal are shown. These were recorded during the spectral diffusion process and sorted by peak energy, plotted in the two-dimensional representation of spectrum versus peak energy, and smoothed in an energy window of 1 meV. As the peak energy shifts to the red, the optical phonon side band increases in intensity and the spectra broaden, giving rise to a funnel-like shape of the plot. Adapted from [27]

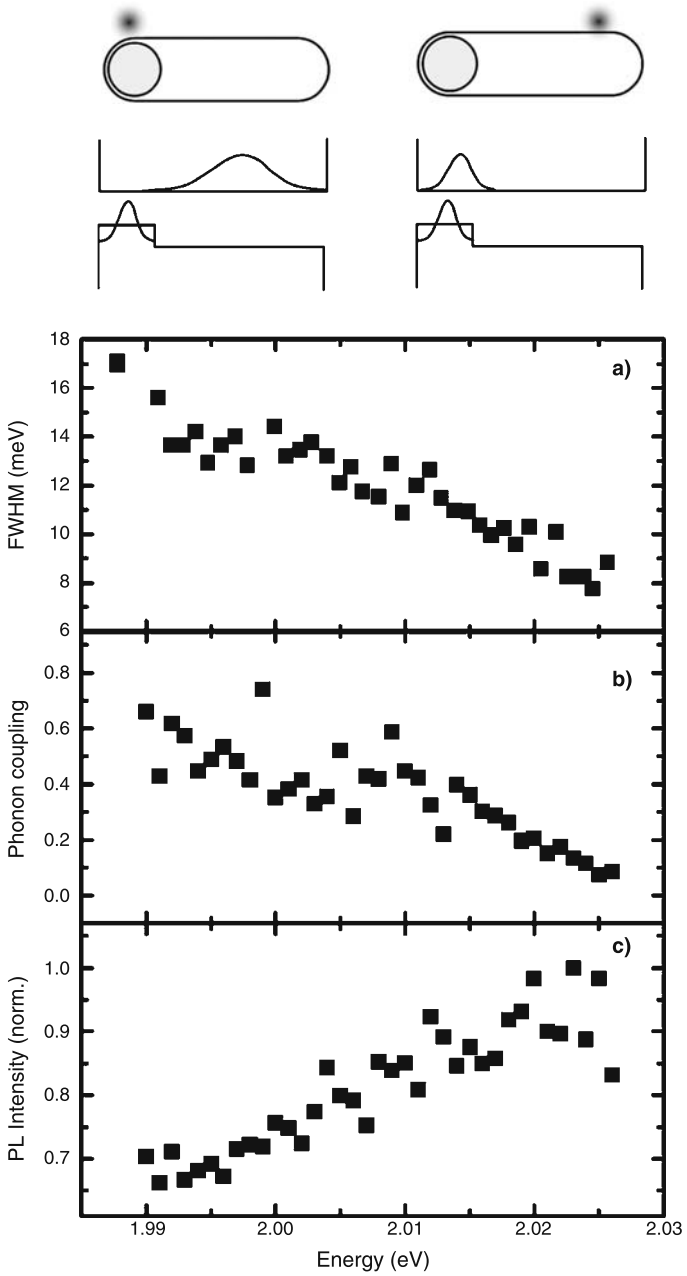

Fig. 8. Correlation between line width, phonon coupling strength and photoluminescence intensity for the sorted spectral trace measured at 5 K and shown in Fig. 7. Sorting of the spectra allows a statistical binning of energetically related spectra *prior* to fitting to the line shape and extracting the line width, peak position, phonon coupling and emission intensity. The scheme reiterates the mechanism responsible for the correlations, explained in more detail in Fig. 5. As the hole is confined to the CdSe core whereas the electron is free to penetrate the CdS shell, surface charges modify the overlap of the electron and hole wave functions, which in turn control line width, phonon coupling, peak energy and photoluminescence intensity. Adapted from [27]

phonon side band in the emission broadens and increases in intensity relative to the zero-phonon line as the emission shifts to the red.

The sorted spectra with the time dimension removed allow a much more facile and accurate extraction of the spectral parameters such as the line width, the phonon coupling strength (the Huang-Rhys factor), and the emission intensity. In addition, the sorted spectra can be smoothed further by binning spectra related in energy, i.e. by taking the spectral average over a sliding window of width of, e.g. 1 meV prior to determining the line width, peak position, etc. by fitting a Lorenzian curve to the spectrum. Figure 8 illustrates the data extracted from a sorted trace of one single particle. Under these conditions, the line width–peak position correlation forms an almost straight line with minimal scatter. As expected from the raw data shown in Fig. 7, the phonon coupling increases monotonously as the emission shifts to the red. Most importantly, the average single particle emission intensity decreases as the emission shifts to the red. All three of these observables are perfectly consistent with the simple surface charge model put forward above and reiterated in the cartoon in Fig. 8.

Charging in quantum dots is known to influence the transition energy. In large, vapour phase-grown quantum dots, charged exciton transitions become visible [75, 76]. In smaller colloids, charging can vastly promote Auger recombination, thereby leading to a quenching of the emission. This phenomenon has been studied intensively using time-resolved pump-probe spectroscopy [77]. Auger recombination has also been made responsible for the blinking of the fluorescence of single nanocrystals [56]. If a charge carrier is ejected from the nanocrystal following photoexcitation, the particle becomes charged, and consequently non-radiative Auger recombination competes with spontaneous emission [78]. If, however, the rate of spontaneous emission is accelerated by, for example, placing the nanocrystals on suitable plasmonic substrates which enhance electromagnetic coupling and therefore the radiative rate [79], emission from the charged exciton can become visible. It is important to distinguish between discrete charging events *within* the quantum dot and continuous redistribution of charges in the *vicinity* of the excitonic species. As demonstrated by Neuhauser et al., a blinking event in the nanocrystal emission correlates with a discrete spectral jump, whereas continuous spectral fluctuations occur at almost constant emission intensity [56]. The elongated nanocrystals allow a more detailed quantification of the role of surface charge fluctuations, i.e. overall changes in the charge of the nanocrystal. The net magnitude of surface charge need not change, but merely its position, in order to influence the emission intensity of the single particle.

The spectral meandering can be further analyzed by returning to the raw data traces. By making the differentiation proposed by Neuhauser et al. [56], we can identify the mean spectral shift between subsequent measurements $\Delta E = E_{\mathrm{peak},n+1} - E_{\mathrm{peak},n}$ and associate this with either a blinking event or a period of constant emission intensity. The spectral shift ΔE is plotted in a histogram. As there are long periods in the emission which are uninterrupted by an intermittency, the statistics are significantly better for the continuous spectral drift (the spectral jitter) than for the discrete spectral changes (the spectral jump). Figure 9 displays histograms for these two cases as derived from one single fluorescence trace of an individual particle (the 5 K trace shown in Fig. 3). As expected, the spectral jump

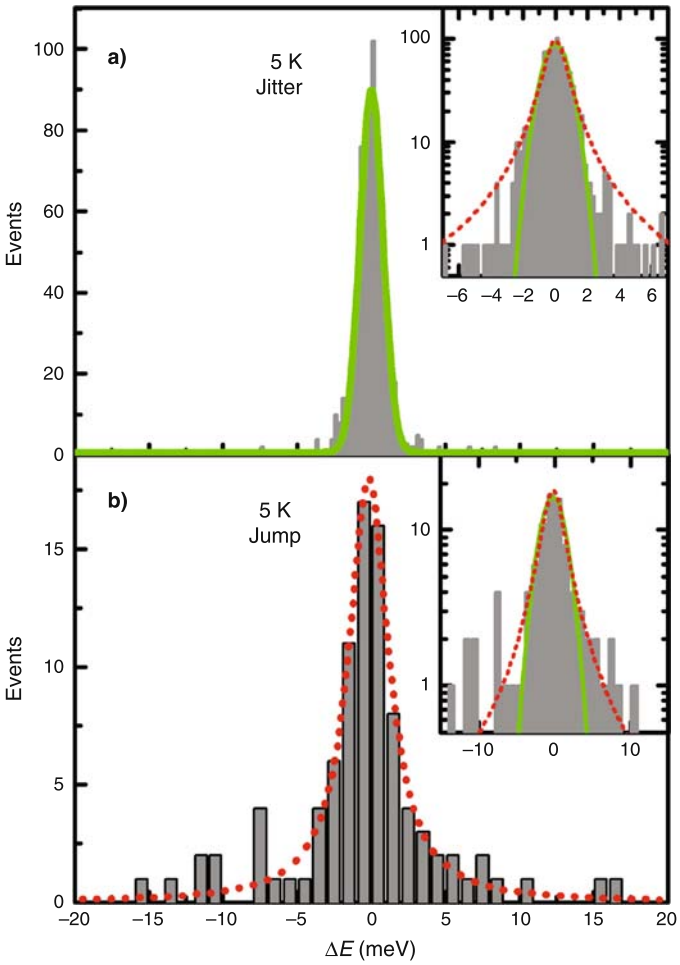

Fig. 9. Spectral diffusion statistics of the photoluminescence trace shown in Fig. 3a. The histograms illustrate the difference in energy $\Delta E = E_{\text{peak},n+1} - E_{\text{peak},n}$ between two subsequent spectral peaks recorded in the trace. **a** Overall trace consisting of 800 events. **b** Events interrupted by fluorescence intermittency (total of 90). The insets show the histograms on a logarithmic scale with a Gaussian (solid line) and a Lorenzian (dotted line) superimposed. Adapted from [27]

histogram is significantly broader than the spectral jitter histogram. A Gaussian function is superimposed on the spectral jitter histogram, which clearly provides a good match. In contrast, the spectral jump histogram appears to be more readily described by a Lorenzian function. The insets show the same histograms on a logarithmic scale, with both Gaussian and Lorenzian functions superimposed. These results illustrate that spectral diffusion in such nanoscale emitters follows a universal distribution of events. Both jump and jitter distributions increase slightly with increasing temperature (as the temperature is raised from 5 to 300 K), but depend strongly on the incident power [27, 45]. Whereas the jump distribution appears to follow a sublinear dependence on excitation density, the spectral jitter increases

linearly [27]. The intensity dependence illustrates that spectral diffusion is a primarily optically driven process [63], resulting from the dissipation of excess photon energy, i.e. the energy difference between the absorbed and emitted photon.

The spectral jitter, which is resolvable on the time scale of 1 s of the experiment, is most likely related to the line width of the single particle spectrum and thus to random spatial fluctuations or oscillations of the surface charge density [64]. The overall histogram of the spectral jitter should therefore contain information on where the surface charge responsible for the quantum-confined Stark effect is located with respect to the exciton in the nanoparticle core. Assuming that the random spatial fluctuations of the surface charge in time, which are responsible for spectral broadening, are independent of the actual location of the charges on the nanocrystal surface, the width of the spectral jitter histogram itself should correlate with the overall spectral red shift. The underlying assumption appears reasonable as the fluctuations in surface charge are most likely due to a redistribution of the population of trap states [80, 81], which should exhibit comparable kinetics along the long axis of the nanoparticle. The way to test for evidence that spectral broadening originates from spectral jitter on time scales which cannot be resolved by the experiment is to study the spectral jitter distribution within different regions of the line width–peak position correlation. Figure 10a shows a typical correlation, which was arbitrarily dissected into three regions. Within these three spectral regions, the spectral jitter histogram is extracted, using the methodology discussed above. Figure 10b displays the spectral jitter histograms for the three regions, superimposed with Gaussian functions. It is clearly seen that as the emission shifts to higher energies, the individual spectral lines narrow, but so does also the actual spectral jitter distribution. The mean spectral shift from one measurement to the next is reduced as the emission moves to the blue. The higher energy emission corresponds to surface charges located at the greatest distance to the emitting core. As the surface charges move closer, the same random spatial fluctuation leads to a greater spectral shift ΔE from one measurement to the next. The closer the surface charges are to the emitting core, the greater the effect of a slight lateral redistribution of the charges on the transition energy will be. Consequently, the further away the charges are from the core, the more uniform the spectral jitter appears. Figure 10c shows the histogram of the most distant region labelled “3”, plotted on a logarithmic scale. The distribution is accurately described by a Gaussian function over two orders of magnitude in event frequency, illustrating that the local fluctuations in electric field responsible for the emission dynamics are purely random in nature.

The elongated shape of the nanoparticle therefore allows a direct spatial tracking of surface charges, leading to correlations of peak position, line width, phonon coupling strength, emission intensity, and spectral jitter. An optical technique, which is, in principle, limited to a spatial resolution of a few hundred nanometers, can

Fig. 10. Dissection of the spectral diffusion of a single nanocrystal at 5 K into three regions, depending on the magnitude of the Stark effect. **a** The line width–peak energy correlation appears continuous and is arbitrarily divided into three equally large regions. **b** Spectral jitter ΔE histograms of the continuous spectral diffusion (blinking events and subsequent discrete spectral jumps were discarded) of the three regions indicated in panel **a**. **c** ΔE distribution of Sect. 3 shown on a logarithmic scale with a Gaussian superimposed, which clearly describes the histogram over two orders of magnitude. Adapted from [27]

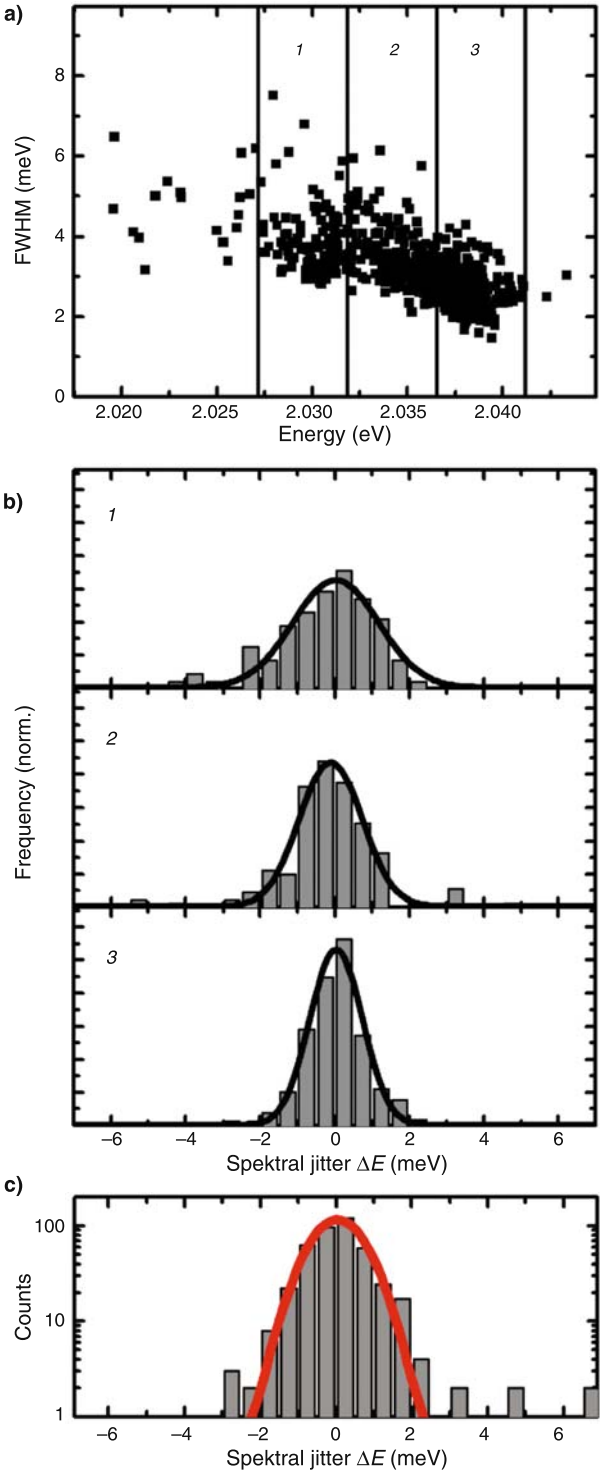
a)
1
2
3
FWHM (meV)
0
2
4
6
8
2.020
2.025
2.030
2.035
2.040
Energy (eV)
b)
1
2
3
Frequency (norm.)
–6
–4
–2
0
2
4
6
Spektral jitter ΔE (meV)
c)
Counts
1
10
100
–6
–4
–2
0
2
4
6
Spektral jitter ΔE (meV)

therefore be used to derive information on charging-related phenomena on length scales of a few nanometers. Random spectral diffusion need not necessarily be a detrimental thing. As discussed below, it can influence excitation energy transfer. The spectral jitter has also been used in quantum optical experiments to drive the excitonic transition in and out of resonance with a photonic mode, providing signatures of strong exciton–photon coupling in a single emitter [82].

An open question is how the clear spectral dynamics correlate with the fluorescence lifetime of single nanocrystals. It is conceivable that spatial redistribution of surface charge leads to a change in both radiative and non-radiative decay rates of the single nanocrystal [83]. Time-resolved fluorescence spectroscopy will provide ultimate insight into how the wave function overlap of the exciton is modified by external charges, and most importantly whether changes in surface charge density do modify non-radiative decay dynamics. Most of the present investigations do indeed suggest that blinking events correlate with a shortening of the fluorescence lifetime due to an increase in non-radiative decay [84–87], but to date it has not been possible to correlate this directly with the low-temperature fluorescence spectroscopy.

5. Universal spectral fluctuations in nanoscale systems

The spectral fluctuations observed in the single nanoparticle emission suggest some level of generality, so the question naturally arises whether similar fluctuations can be observed in different material systems. The fluctuations most likely originate from a spatial redistribution of charges, i.e. an optically driven electron transfer process. Dynamic electron transfer phenomena are well known from photochemical studies of molecules and surfaces [88], but are also observed in the noise of electrical transport measurements on small systems [89, 90]. Under certain conditions single molecules have been found to exhibit similar blinking dynamics to nanocrystals [91], suggesting some unifying behaviour. Interestingly, very similar spectral fluctuations are observed in the emission of a single chain of the conjugated polymer MEH-PPV [92, 93], a prototypical material system used in organic light-emitting diodes and photovoltaic devices. The excited state structure of such a macromolecule is very different to that of a quantum dot. The excitation in the polymer is highly anisotropic, the intramolecular bonds are covalent rather than ionic, and the dielectric constants are much lower so that the Coulombic interaction between electron and hole is stronger. Figure 11 displays the fluorescence jitter of such a single-polymer molecule, emitting in the spectral range around 530 nm at 5 K. Discrete spectral jumps are observed along with a pronounced spectral jitter of the primary transition line, which has a width of approximately 0.5 nm. The histogram of spectral diffusion, which does not differentiate between jump and jitter as in the case of Fig. 9, exhibits a pronounced Gaussian peak corresponding to the continuous spectral jitter. Side lobes are observed around ± 20 meV, which result from the discrete spectral jumps. The histogram of spectral diffusion is evidently similar to that observed for the nanocrystals, but the typical jumps are approximately twice as large.

On the one hand, the spectral dynamics of single nanocrystals do not appear to depend strongly on the immediate dielectric environment [24, 69], and are merely controlled by the immediate density of surface charge on the nanoparticle. On the

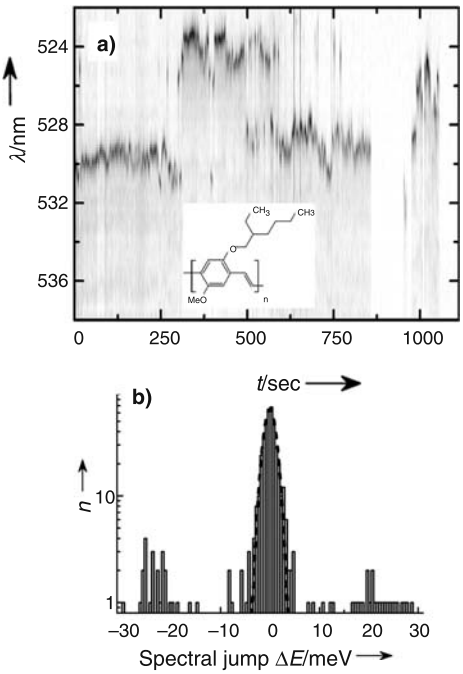

Fig. 11. Spectral diffusion in single chains of a conjugated polymer. **a** Single chain fluorescence of the polymer MEH-PPV as a function of time at 5 K, measured with a temporal resolution of 2 s. The emission spectrum is shown in a grey scale representation with darkening tones corresponding to increasing intensity. Switching between seemingly alike emissive states is observed along with a strong spectral jitter. By fitting a Lorenzian line to the individual spectra, both the spectral width and the spectral position can be extracted. **b** Histogram of the energy difference ΔE between two consecutive spectra, shown on a logarithmic scale. The distribution is accurately described by a Gaussian of width 2.4 meV. The large jumps in the spectral trace lead to a second group of events at ± 22 meV. Adapted from [93]

other hand, very similar temporal fluctuations are observed in rather different distinct nanoscale light sources, such as the conjugated polymer MEH-PPV. An interesting comparison can be drawn between the polymer and the nanocrystal. In effect, the polymer also possesses surface charge, harboured by the backbone substituents which interface the conjugated π-electron system with the outside world. One way to test this hypothesis is to carry out Stark spectroscopy of single chains by monitoring the molecular fluorescence under an electric field [94]. For the case of MEH-PPV, this experiment reveals that a linear Stark shift of the emission, indicative of the presence of a permanent polarisation, is only observed when the highly polarisable π-system is oriented orthogonal to the external electric field. The conclusion drawn from this result is that the polar alkoxy groups linking the side chains to the conjugated backbone induce a permanent polarisation within the molecule. Molecules without such polar substituents display a smaller Stark shift [94]. Interestingly, spontaneous fluctuations of the magnitude of the Stark shift, i.e. the magnitude of polarisation of the molecule, have also been observed for some material systems [95], indicating dynamic charge redistribution events. In general, the polarisation of a nanoscale entity is an extremely important parameter in understanding its interaction

with individual charges and external electric fields. Conjugated polymers, for example, are used in light-emitting diodes, field-effect transistors, and photovoltaic devices. In a light-emitting diode, the question is how a charge carrier is actually injected from the electrode into the highest occupied or lowest unoccupied orbital of a molecule. Over two decades of research it has become clear that the injection efficiency is not merely defined by an offset of the energy of the molecular orbital with respect to the work function of the metal [96]. A dipole, oriented orthogonally to the polymer chain, induces an internal electric field which can either increase or reduce the externally applied field. Injection of charge carriers from the electrodes therefore only occurs into suitably oriented molecules. The effect is equally important in field-effect transistors. More so, such devices are based on a field-induced (electrostatic) polarisation of the medium. If the semiconducting layer is already polarised due to chemical substitutions or the formation of the trapped charges within the vicinity of the conjugated segment, an electric gate field will not be able to switch the conductivity sufficiently. Finally, molecular polarisations could be rather beneficial to charge separation, the elementary process in photovoltaic devices. Molecular semiconductors are characterised by vast exciton (electron–hole) binding energies, typically of order 0.5 eV [97]. Dipoles may promote carrier dissociation and then guide the optically generated charges on a suitable pathway towards the electrodes under the action of the built-in field.

These examples serve to illustrate the subtle complexity of describing the interaction of a nanoscale electronic system with the outside world, but also underline the occurrence of some universal signatures. Noise arising from random charge fluctuations is important in transport spectroscopy of semiconductor nanosystems [90] and can even induce decoherence in quantum information systems such as Josephson junction qubits [98]. The random spectral fluctuations, associated with charging phenomena, are therefore relevant to a wide range of physical systems, and even find analogues in biophysical relaxation dynamics [99].

6. Control of single particle emission by electric fields

The previous discussion illustrated that the remarkable optical dynamics of single quantum dots can be understood in terms of temporally varying electric fields. However, quantitative confirmation that it is indeed electric fields and the quantum-confined Stark effect which are responsible for the spectral dynamics, can only be derived from actually applying external electric fields to the particles. This approach was initially taken by Empedocles and Bawendi in 1998, who demonstrated that the spontaneous spectral shifts observed in the fluorescence can be reproduced entirely by external electric fields [64]. Similar effects have also been discussed for epitaxially grown quantum dots [100]. The authors defined two types of local charge effects: periodic fluctuations in surface charge; and polarisation of the particle through (semi-)permanent rearrangement, i.e. generation or annihilation, of surface charge [64]. The unique system of elongated semiconductor nanocrystals with broken dimensionality now allows us to address the question of the role of particle shape in the fundamental interaction with electric fields [101]. As will be shown later on, this interaction can then be exploited to design a new category of energy transfer-

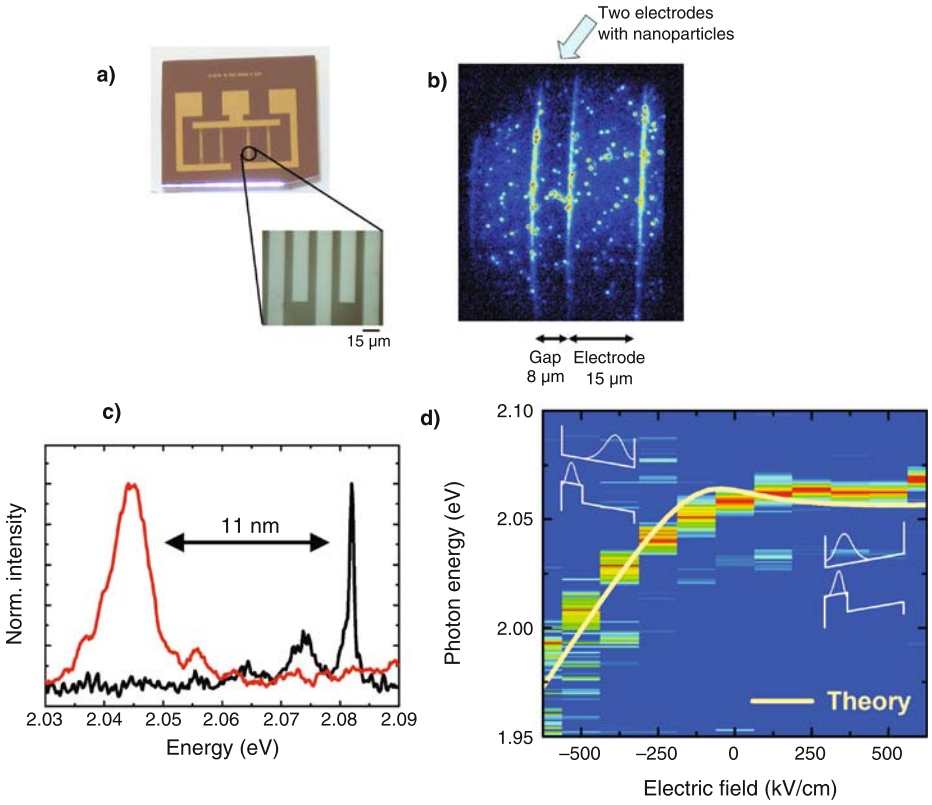

Fig. 12. The quantum-confined Stark effect in the emission of single elongated nanocrystals. **a** Photograph of the interdigitated finger electrode structure used to apply large lateral electric fields of up to 0.5 MV/cm. **b** Image of the electrode structure as seen beneath the fluorescence microscope. The spots correspond to emission from single nanocrystals. To study field effects, nanocrystals are chosen which are located in between two electrode fingers, which are clearly identified in the image through enhanced light scattering. **c** Quantum-confined Stark effect in the single particle emission at 5 K. The normalized emission spectra of a single nanocrystal in an external electric field show a large shift to the red by approximately 11 nm as the bias applied is changed from +200 to –500 V. **d** Normalised fluorescence spectra as a function of electric field applied, indicating a highly asymmetric electric field effect due to the asymmetry of the nanoparticle shape and composition. Negative fields can move electron and hole apart in the structure, as indicated in the inset showing the band structure and the calculated wave functions, whereas positive fields barely modify the confinement. The solid line shows the results of calculations using the effective mass approximation in a selfconsistent field method. Adapted from [101]

based optoelectronic devices [102]. In addition, it will be shown that Stark spectroscopy provides direct insight into the shape of the nanoparticle, information which is hard to access by other means.

Figure 12 summarizes the experimental approach to perform Stark spectroscopy on single elongated nanocrystals. The nanocrystals are spin-coated in their polymer solution onto an array of interdigitated finger electrodes, a photograph of which is shown in Fig. 12a. These fingers have a spacing of 8 µm and enable the application of uniform electric fields of over 0.5 MV/cm. It is not entirely trivial to switch from the conventional microscope samples to the finger electrodes due to the different surface

wetting properties of the lithographically prepared electrodes, requiring an adjustment of nanoparticle concentration and spinning speeds. Figure 12b illustrates a microscope image of the nanoparticles deposited on top of the finger electrodes. Fluorescence spots are observed both between the electrodes and on top of the aluminium fingers. As one would expect from spin-coating a highly dilute, non-viscous solution, accumulation of particles occurs near the edges of the fingers. Stark spectra are only considered from particles situated at the centre between the two electrodes. Figure 12c displays a typical Stark shift spectrum, recorded under an applied bias of +200 V (black) and −500 V (red). Evidently, the electric field can strongly modulate the fluorescence spectrum, leading to a shift of the emission maximum by over 11 nm. As will be shown later on, this is a significant spectral shift, many times the transition line width, which can be exploited in applications. In contrast to spherical nanocrystals, which typically exhibit a small quadratic (isotropic) Stark shift superimposed on a strong linear Stark shift depending on the polarity of the surface charge [64], suitably oriented elongated nanocrystals generally display a highly anisotropic Stark effect, as shown in Fig. 12d. A spectral shift is only observed for negative electric fields, not for positive fields. This effect is a direct consequence of the spatial asymmetry of the nanoparticle, which outweighs any influence of polarising surface charges. The quantum-confined Stark effect leads to a red shift of the excitonic transition when the electron (or hole) wave function can penetrate the quantum-confining barrier layer. This is only the case for negative fields in the example given. There is a substantial energetic barrier for holes between the CdSe core and the CdS shell, whereas the electron is effectively isoenergetic in the two materials. Application of a negative field for a particle with the CdSe core pointing towards the cathode results in the electron within the exciton being pushed out of the CdSe core. This lowers the quantum mechanical confinement and results in a spectral red shift. Reversal of the field does not alter the transition energy significantly, as the electron and hole cannot be pushed arbitrarily close together due to an increase in the correlation energy with decreasing carrier spacing [101]. A relatively straightforward effective mass Hamiltonian, solved using an iterative selfconsistent field method and described in [101], reproduces the experimental observations accurately as shown by the solid line in Fig. 12d. Some approximations have to be made in this comparison, however, as the surrounding matrix and the substrate partially screen the electric field. The effective electric field experienced by the particles is therefore somewhat smaller than the mere ratio of the potential applied to the electrodes and the electrode separation. The sketches inset in Fig. 12d illustrate the calculated wave functions of electron and hole in the nanoparticle. A direct consequence of the separation of electron and hole through application of an electric field is the reduction in wave function overlap, which determines the radiative rate. Assuming that the non-radiative rate remains constant, reduction in the wave function overlap should therefore result in a decrease in emission intensity. Note that the reduction in emission intensity was also described above for the case of spontaneous rearrangements of surface charges, and could clearly be correlated with the change in emission wavelength as shown in Fig. 8 [27]. The externally induced spectral and intensity fluctuations are, however, significantly larger than the spontaneously occurring phenomena.

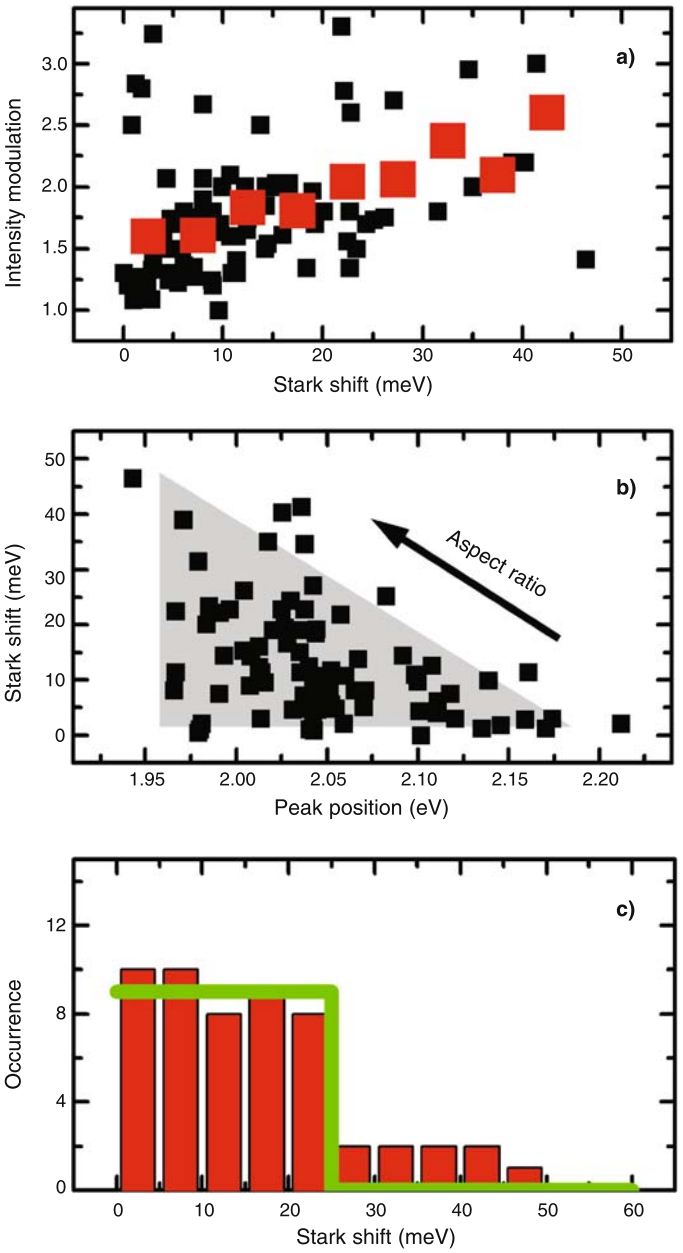

Fig. 13. Statistics of the quantum-confined Stark effect for 88 single nanoparticles. **a** Correlation between the maximum Stark shift and the overall intensity modulation (black squares). Large squares indicate 5 meV average bins. **b** Statistical distribution of the QCSE magnitude as a function of emission wavelength. The grey triangle highlights the increase of the QCSE with the decrease in emission energy. This decrease in energy corresponds to an increasing aspect ratio and thus an increasing electron penetration volume. The triangular scatter arises because of the random particle orientation. **c** Frequency of occurrence of a particular Stark shift illustrating an isotropic spatial distribution of the particles with respect to the field. The green line indicates the statistically expected distribution. Adapted from [101]

The average spectral shifts per unit field are several times greater for the elongated nanoparticles than for spherical particles [64]. As the elongated particles are larger, the overall effect of surface charge on the spectral characteristics is weaker than for spherical particles, in particular when compared to core-only spheres [64]. The influence of a large external electric field can therefore be described accurately without needing to include surface charge effects, which only serve to induce a particular electric field offset to the spectral shift. Nanoengineering of the electronic structure of the particle allows us to induce a new functionality, in this case an enhanced quantum-confined Stark effect.

The Stark effect is anisotropic in these anisotropic particles and can be used to extract information on the shape and shape distribution of the nanocrystals. Although transmission electron microscopy provides access to the shape distribution of the particles, it cannot yield information on the microscopic distribution in composition and in particular on three-dimensional shape. Stark spectroscopy probes the polarisability of the nanoparticle, which is a three-dimensional quantity directly related to the volume of the particle. Figure 13 provides detailed statistics of the modulation of single particle photoluminescence by an electric field of 350 kV/cm. The electric field leads both to a spectral shift (to the red) and to a modulation in intensity (a reduction), defined as I_{max}/I_{min}. For the 88 particles shown in the figure it is apparent that the intensity modulation correlates directly with the Stark shift. The further electron and hole can be moved apart within the nanocrystal, the larger the Stark shift, the greater the intensity modulation. The large squares in the figure indicate the average binned over a region of 5 meV to reduce the statistical scatter in the data points. The scatter in the Stark shift and in the intensity modulation can have two origins: either the particles are not aligned suitably with respect to the electric field; or the polarisable volume varies strongly from particle to particle. These two effects can be distinguished. The polarisable volume must correlate with the particle size, which is in turn defined by the aspect ratio. The larger the particle, the weaker the overall quantum confinement, the further in the red emission occurs. Figure 13b provides a plot of the observed Stark shift against the zero-field fluorescence peak position, which is expected to correlate directly with the size of the nanoparticle. It is seen that the larger the particle is (i.e. the further in the red the emission occurs), the greater the maximum observed Stark shift is. However, the particles are oriented randomly with respect to the electric field, so if a particle has its long axis orthogonal to the field only a very weak spectral modulation will be recorded [101]. Consequently, the scatter of points in the plot is described by the shape of a triangle. To address the question of orientation, we can now consider the most polarisable particles, i.e. the particles in Fig 13b with a transition energy smaller than 2.05 eV. Figure 13c shows a histogram of the frequency of a particular Stark shift for these largest particles. The histogram resembles a flat step, switching at a Stark shift of 25 meV. The histogram can be accurately reproduced by semiempirical calculations [101] by assuming a random distribution of the particles in the plane with respect to the electric field, as indicated by the green line.

Semiconductor nanocrystals are highly polarisable so that their emission characteristics can be controlled by external electric fields, making them suitable building blocks for optoelectronic devices. Engineering of the shape breaks the

particle symmetry so that only a certain subset of nanoparticles respond to electric fields. On the one hand, one would expect the highly anisotropic Stark shifts to average out in the ensemble; no change of photoluminescence with electric field should be observed in a bulk film [64]. However, temporal modulation of the electric field allows one to pick out a particular shape subset of nanocrystals, namely just those nanocrystals which display the strongest electric field response. This enables fluorescence modulation and the Stark effect to be observed at room temperature in the ensemble [103]. In brief, a thin film consisting of a blend of nanocrystals in an inert polymer matrix is deposited between two vertical electrodes. Application of an electric field quenches the fluorescence of the ensemble, as is readily observed. Time-resolved (gated) spectroscopy allows one to study both the intensity and the spectral dynamics. If the electric field applied to the device is removed after a duration of one microsecond, much of the initially quenched fluorescence is recovered, leading to a pronounced fluorescence burst. The anisotropic shape of the nanocrystals therefore provides a pathway to storing excitons in semiconductor nanostructures, over time scales well beyond the typical durations of radiative decay. This is made possible by reversibly converting the direct, emissive exciton into an indirect, dark state [104]. Interestingly, the fact that the temporal gating technique accesses a particular subset of nanocrystals allows the observation of the quantum-confined Stark effect in the ensemble emission at room temperature [103]. This room-temperature demonstration of an electric field effect illustrates the power of low temperature single particle spectroscopy in identifying new application areas of nanoscale semiconductors.

7. Single nanocrystals as a probe of excitation energy transfer in disordered systems: the FRET gate

Much of the research interest in semiconductor nanocrystals has been driven by their characteristics as bleach-resistant nanoscale light beacons [105]. Single molecule fluorescence opened an entirely new dimension to the physical characterisation of biological systems [106] and has enabled experimenters to observe the hybridisation of single DNA strands, folding of proteins, and even the nature of motion of various molecular motors [107, 108]. Optical experiments in the limit of linear excitation are confined to length scales comparable to the wavelength of light, dimensions much larger than a typical displacement of a molecular entity. However, by studying the combined optical response of two fluorescent species, the spatial resolution of optical microscopy can be enhanced dramatically [109]. Labelling a DNA strand with two different fluorescent molecules, a donor and an acceptor, can provide information on hybridisation of the DNA. Provided an electronic resonance exists between the two labels, i.e. the donor can pass its excitation energy on to the acceptor given sufficient spectral overlap between the donor emission and the acceptor absorption, a small rearrangement in the spatial orientation or separation of the donor with respect to the acceptor will result in a substantial change in the acceptor emission intensity. Such experiments assume that donor and acceptor labels can be excited selectively, i.e. that the donor can be excited optically without photopumping the acceptor. On the other hand, the donor should absorb as much light

as possible to maximize the fluorescence of the beacon while minimizing residual and undesirable background fluorescence. Semiconductor nanoparticles have very broad absorption spectra, with the absorption increasing continuously as the wavelength of light is reduced below the optical gap. In addition, nanocrystals are larger than most molecular dyes and can hence absorb more light energy per particle. Semiconductor nanocrystals are therefore interesting as labels for biophysical investigations [110–115]. As will be discussed in the following, the FRET properties of nanocrystals can even be used to learn more about the nanoparticle material characteristics and its interaction with the surrounding.

FRET can be likened to transmission and reception of radio waves on the nanoscale. Only when transmitter and receiver are in resonance, i.e. the transmitting and absorbing antennae and oscillating circuitry are tuned to have the same frequency, can energy and information be transferred. In addition, FRET is a near-field phenomenon. As light passes through a block of glass and is reflected at the boundary to air due to total internal reflection, only the travelling part of the light-field is considered. However, press a second block of glass against the first block of glass, and light transmission through the thin air gap will be observed. As in the analogy of quantum mechanical tunnelling, the solution to Maxwell's equation simply becomes real, i.e. exponentially decaying, in the region of total internal reflection. An index-matched material can enable the wave solution to become imaginary and therefore propagating again, in effect tunnelling the light across a non-propagating gap. Electrodynamic interactions over this gap are extremely sensitive to distance. Efficient coupling between transmitter and receiver can occur over the gap, i.e. for the real, evanescent wave solution of the wave equation.

Most considerations of FRET in the past have only taken the spectral overlap between donor emission and acceptor absorption in the ensemble into account. FRET is, however, a fundamentally microscopic process. A complete understanding of FRET therefore requires that the microscopic spectral overlap between the absorption of one single acceptor unit and the emission of one single donor unit are considered. As discussed above, going from the ensemble of nanocrystals to single particles and lowering the measurement temperature dramatically reduces the transition line width. If nanocrystals are used as donors in a FRET experiment, one may expect the strength of resonant incoherent dipole–dipole coupling to change with temperature. This change will depend on the properties of the acceptor transition. Typically, one may expect that the absorption line width of a single acceptor will also narrow with decreasing temperature. One single donor will therefore not be able to pass excitation energy to any arbitrary acceptor, but only to proximal acceptors with suitable transitions. The density of these acceptors will decrease as the temperature is lowered. On the other hand, as the temperature drops, FRET becomes much more selective and can therefore be used to probe a certain subset of the ensemble. Fortunately, the electronic transitions of nanocrystals are tuneable through the quantum-confined Stark effect. We therefore expect to be able to push an individual donor–acceptor pair in and out of resonance.

Figure 14 summarizes the concept of electrically controllable Förster-type energy transfer between a single semiconductor nanorod and a suitable dye acceptor [102]. As FRET becomes selective at low temperatures to a small subset of the acceptors,

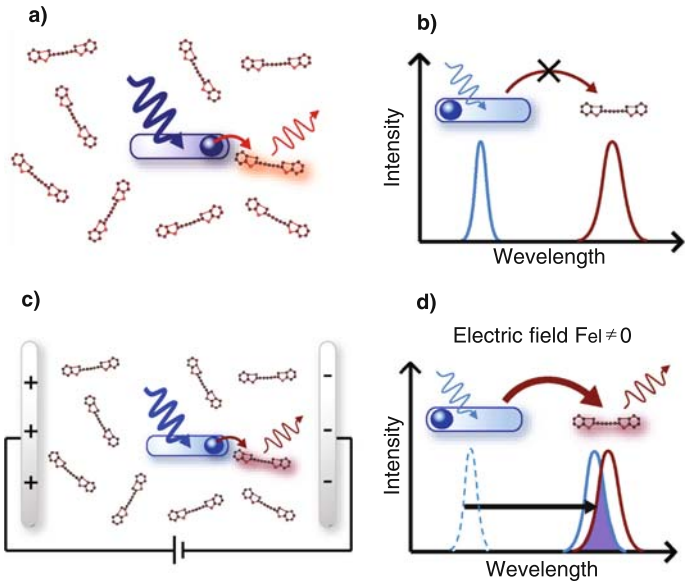

Fig. 14. Electrical control of energy transfer in a single FRET couple consisting of an absorbing dye molecule and an emitting nanocrystal. **a** The nanocrystals are dispersed in a dye film so that the nanocrystal concentration by far exceeds the concentration of dye molecules. Each nanocrystal should therefore, in principle, have an adjacent acceptor molecule. **b** At low temperatures, however, the electronic transitions of donor and acceptor are too narrow to enable a sufficient spectral overlap, required for efficient FRET. **c** Application of an electric field to the nanocrystal–dye mixture can facilitate FRET by shifting the emission of the nanocrystal into resonance with the absorption of an adjacent dye molecule **d**. Adapted from [102]

we can consider the nanocrystal donor in a mixture with dye molecules at higher concentration. The nanocrystal donor with the much larger absorption cross section (in the present case, for the choice of excitation wavelength of 458 nm and the cyanine dye derivative used as an acceptor, the absorption ratio is over 1:1000) acts as a form of excitonic optical nanoantenna, absorbing the incident laser radiation and passing it on selectively to a dye molecule in its vicinity [116]. The nanocrystal nanoantenna is therefore able to pick a single dye molecule out of a seemingly homogeneous film of dye molecules, effectively forming a subdiffraction optical probe addressed in the optical far-field. A typical nanocrystal will not display suitable spectral overlap with the dye emission as the transitions narrow at low temperature, as indicated schematically in Fig. 14b. Application of an electric field can remedy this deficiency, driving the nanocrystal donor into resonance with the dye acceptor (Fig. 14c, d) so that electrically controlled FRET occurs.

The experimental implementation of this FRET switch is demonstrated in Fig. 15. A periodic electric field is applied to a mixture of nanocrystals and dye molecules. Figure 15a shows the modulation of the fluorescence of a nanocrystal in a plot of fluorescence wavelength against time. Turning the electric field on and off leads to a red shift of the nanocrystal emission by approximately 10 nm. This spectral shift can drive the nanocrystal into resonance with the absorption of a nearby dye acceptor. Figure 15b displays the fluorescence of such a dye molecule as a function of time,

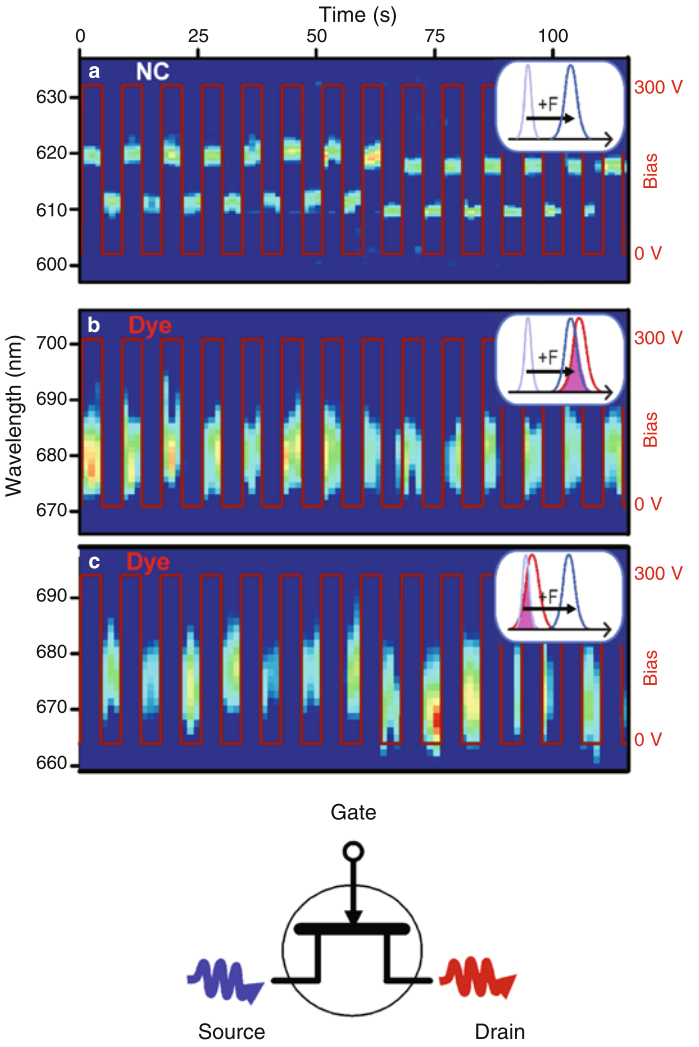

Fig. 15. Electrical control of energy transfer. **a** A periodically modulated electric field shifts the emission a typical nanocrystal by 10 nm. This shift in emission spectrum controls the FRET efficiency from nanocrystal to dye, depending on the zero-field spectral overlap of nanocrystal donor and dye acceptor. **b** If the adjacent dye molecule is not in resonance with the nanocrystal emission at zero-field, the applied electric field can switch FRET on, thereby making the dye fluorescence appear. Note that the dye spectrum is distinct from the nanocrystal spectrum: it is shifted to the red to approximately 680 nm and significantly broadened. **c** If donor and acceptor are in resonance at zero-field, application of an electric field can destroy the resonance, thereby turning the acceptor emission off. The overall phenomenon corresponds to a form of a field-effect switch, in which the electrical gate – the Stark effect – controls the excitation energy flow from source (nanocrystal) to drain (dye molecule). Adapted from [102]

recorded at a temperature of 50 K. Note that the dye spectrum is significantly broader than the nanocrystal spectrum and shifted to the red by over 60 nm. In contrast to the nanocrystal emission, the dye luminescence does not exhibit any spectral shift with applied bias. However, the dye emission is switched on and off depending on the

magnitude of the electric field. Application of the field drives the nanocrystal into resonance with the dye so that excitation energy is transferred – the dye molecule lights up. As in the case of the nanocrystals (see Fig. 2a), every single dye molecule has a distinct transition energy as every molecule has a slightly different microscopic conformation which controls its electronic structure. A certain dye molecule may therefore turn out to be in resonance with the nanocrystal donor in the absence of an electric field. In this case, which is illustrated in Fig. 15c, the electric field drives the nanocrystal out of resonance with the dye acceptor; the dye fluorescence vanishes under application of a field.

This concept of voltage-switchable energy transfer can be thought of as a nanophotonic transistor in the form of a FRET gate, as illustrated in Fig. 15. A voltage gate, the quantum-confined Stark effect, controls the flow of excitation energy from the source (the nanocrystal absorber of external radiation) to the drain (the dye emitter of radiation to the outside world). It is now up to materials chemists to devise routes of linking multiple such logic elements to each other to construct versatile nanophotonic circuitry. This will be an interesting challenge, as it is already hard to link precisely one molecule to one single nanocrystal [117], which is physically much larger. As an aside, this FRET gate also constitutes an exquisite sensor of the local dielectric environment, which controls the electric field experienced by the nanocrystal. The FRET functionality in effect serves to amplify the quantum-confined Stark effect: the spectral shift of the nanocrystal by $\sim$10 nm results in a shift of the emission of the hybrid couple from the nanocrystal to the dye molecule, i.e. by over 60 nm. The recent demonstration of the possibility to sense the photonic environment, i.e. the photonic mode density, with a single nanocrystal [118], provides an additional avenue of applications for tuneable FRET couples. It is also worth noting that electrical pumping of single nanocrystals was recently demonstrated [119, 120]. In combination with lateral electric fields which tune FRET, such a device could offer a voltage tuneable light-emitting diode for single photons on demand.

The FRET gate can also be used to gain insight into the disorder limitation of energy transfer, which is as important in biological light-harvesting systems as it is in synthetic energy conversion devices. The electric field can effectively be used to map out the inhomogeneous broadening of the local acceptor ensemble. Interestingly, spectral diffusion as discussed above can reduce the constraints on resonance matching of donor and acceptor. In addition, thermally activated spectral broadening (which may be due to increased electron–phonon coupling, accelerated spectral diffusion, or even accelerated electronic dephasing) can enhance microscopic dipole–dipole coupling [2]. It was found that the FRET gate experiments were ideally performed at temperatures around 50 K. Below this temperature, the electronic transitions particularly of the acceptor become too narrow so that spontaneous spectral diffusion leads to a random temporal modulation of the FRET efficiency [116]. For higher temperatures, on the other hand, the Stark shift becomes too small with respect to the transition line width, diminishing the FRET gate effect.

It is often assumed that spectral overlap in the ensemble is a sufficient criterion for FRET to occur. This is clearly not the case. Increased polydispersity of the particles could readily improve the ensemble spectral overlap. If anything, this would reduce the microscopic density of suitable donor–acceptor pairs, leading to an overall

reduction in FRET efficiency. Biophysical nanocrystal beacon experiments therefore require a careful trade-off between single particle and single molecule line widths of donor and acceptor as well as their spectral separation to optimize the probability of creating a functional FRET couple.

Returning to the original discussion of this chapter, it is interesting to note the influence of spectral diffusion on FRET. Depending on the temperature and the line widths relative to the typical magnitudes of spectral diffusion, a random spectral jitter of either donor or acceptor may increase or decrease FRET. For a case where spectral overlap is generally poor, random spectral fluctuations may sporadically enhance FRET. In an ensemble, these fluctuations in FRET are clearly averaged out, but they directly determine the overall FRET efficiency. A microscopic control over spectral diffusion, which may be achievable through chemical modification of the surface groups, could therefore be of interest to tuning FRET efficiencies of nanocrystals to molecular materials, for example, in hybrid polymer–nanocrystal solar cells [121]. Finally, it is worth noting that electrical control of dipole–dipole coupling in molecular systems [122] and in epitaxially grown quantum dots [123, 124] has been discussed in the context of quantum computing applications. The synthetic versatility of semiconductor nanocrystals certainly merits taking a deeper look at the surprising range of functionality achievable with these systems in terms of applications which may not be immediately apparent – such as quantum computation [125].

8. Conclusions

Semiconductor nanocrystals constitute a fascinating example of nanoscale light sources. The control of physical shape and chemical composition availed by ever increasingly versatile synthetic procedures goes hand in hand with nanoscale optical characterisation techniques. Single particle fluorescence probes the immediate electrostatic environment of the particle, but in turn also provides direct information on the shape of the nanostructure. Studies of single particles directly reveal the intrinsic electronic properties, which are important for describing the electronic transitions with suitable theoretical models [101]. The single particle studies reveal that a significant contribution to spectral broadening of the ensemble arises from spectral diffusion of the individual excitonic transition. This spectral diffusion correlates directly with the shape of the nanocrystal and can be thought of as originating from the spatial redistribution of surface charge [27]. The elementary transition in the nanocrystal is highly polarisable, making electric field modulation possible on the single particle level. These quantum-confined Stark spectroscopic investigations also bear strong signatures of the nanoparticle geometry, promoting Stark spectroscopy to a versatile tool for studying nanoscale shape [101]. The electric modulation of single particle fluorescence constitutes an example of a nanoscale optoelectronic device, where electrical information is encoded onto an optical output. While usable single particle modulators are still a long way off, this remarkable ability to control the electronic properties of a nanoscale light source enables the construction of a unique functional device, the FRET gate, which switches the flow of excitation energy. This proof of principle, which is also important to understand the general disorder limitation of FRET and the way in

which this limitation can be overcome by spontaneous spectral diffusion, points the way to a new class of hybrid nanoscale devices which will exploit the full potential of molecular and colloidal selfassembly. Having demonstrated such novel functionality, which is only made possible by bringing together material constituents with differing individual properties [102], materials chemists are now challenged to develop routes to link different nanoscale FRET gates together to construct logic circuitry. Such building blocks could find applications in both computation and communication, and are particularly interesting for the development of novel dielectric and biophysical nanoscale sensors.

Acknowledgements

The authors are indebted to Klaus Becker, Florian Schindler, Jochen Feldmann, Andrey Rogach and Dmitri Talapin for many stimulating discussions in the course of the research described in this chapter, and express their gratitude to Dmitri Talapin and Horst Weller for the kind provision of the excellent samples used. JML thanks Florian Schindler for illuminating the analogy of spectral jitter in conjugated polymers, shown in Fig. 11. JML thanks Klaus Becker for investigating applications of the quantum-confined Stark effect and realising the FRET gate, described in Figs. 14, 15.

References

[1] Scholes GD, Rumbles G (2006) Excitons in nanoscale systems. Nat Mater 5: 683–696
[2] Jang SJ, Newton MD, Silbey RJ (2004) Multichromophoric Forster resonance energy transfer. Phys Rev Lett 92: 218301
[3] Fleming GR, Scholes GD (2004) Physical chemistry – quantum mechanics for plants. Nature 431: 256–257
[4] Kühlbrandt W (1995) Photosynthesis – many wheels make light work. Nature 374: 497–498
[5] van Oijen AM, Ketelaars M, Kohler J, Aartsma TJ, Schmidt J (1999) Unraveling the electronic structure of individual photosynthetic pigment-protein complexes. Science 285: 400–402
[6] Hofmann C, Aartsma TJ, Michel H, Köhler J (2003) Direct observation of tiers in the energy landscape of a chromoprotein: a single-molecule study. Proc Natl Acad Sci USA 100: 15534–15538
[7] Moerner WE, Orrit M (1999) Illuminating single molecules in condensed matter. Science 283: 1670
[8] Müller JG, Lemmer U, Raschke G, Anni M, Scherf U, Lupton JM, Feldmann J (2003) Linewidth-limited energy transfer in single conjugated polymer molecules. Phys Rev Lett 91: 267403
[9] Brokmann X, Giacobino E, Dahan M, Hermier JP (2004) Highly efficient triggered emission of single photons by colloidal CdSe/ZnS nanocrystals. Appl Phys Lett 85: 712–714
[10] Lounis B, Bechtel HA, Gerion D, Alivisatos P, Moerner WE (2000) Photon antibunching in single CdSe/ZnS quantum dot fluorescence. Chem Phys Lett 329: 399–404
[11] Nirmal M, Dabbousi BO, Bawendi MG, Macklin JJ, Trautman JK, Harris TD, Brus LE (1996) Fluorescence intermittency in single cadmium selenide nanocrystals. Nature 383: 802–804
[12] Stefani FD, Knoll W, Kreiter M, Zhong X, Han MY (2005) Quantification of photoinduced and spontaneous quantum-dot luminescence blinking. Phys Rev B 72: 125304
[13] Stefani FD, Zhong XH, Knoll W, Han MY, Kreiter M (2005) Memory in quantum-dot photoluminescence blinking. J Phys 7: 197
[14] Chung I, Witkoskie JB, Cao JS, Bawendi MG (2006) Description of the fluorescence intensity time trace of collections of CdSe nanocrystal quantum dots based on single quantum dot fluorescence blinking statistics. Phys Rev E 73: 011106
[15] Verberk R, van Oijen AM, Orrit M (2002) Simple model for the power-law blinking of single semiconductor nanocrystals. Phys Rev B 66: 233202
[16] Shimizu KT, Neuhauser RG, Leatherdale CA, Empedocles SA, Woo WK, Bawendi MG (2001) Blinking statistics in single semiconductor nanocrystal quantum dots. Phys Rev B 63: 205316
[17] Pelton M, Grier DG, Guyot-Sionnest P (2004) Characterizing quantum-dot blinking using noise power spectra. Appl Phys Lett 85: 819–821
[18] Kuno M, Fromm DP, Hamann HF, Gallagher A, Nesbitt DJ (2000) Nonexponential "blinking" kinetics of single CdSe quantum dots: a universal power law behavior. J Chem Phys 112: 3117–3120

[19] Kuno M, Fromm DP, Hamann HF, Gallagher A, Nesbitt DJ (2001) "On"/"off" fluorescence intermittency of single semiconductor quantum dots. J Chem Phys 115: 1028–1040
[20] Tang J, Marcus RA (2005) Mechanisms of fluorescence blinking in semiconductor nanocrystal quantum dots. J Chem Phys 123: 054704
[21] Efros AL, Rosen M (1997) Random telegraph signal in the photoluminescence intensity of a single quantum dot. Phys Rev Lett 78: 1110–1113
[22] Pelton M, Smith G, Scherer NF, Marcus RA (2007) Evidence for a diffusion-controlled mechanism for fluorescence blinking of colloidal quantum dots. Proc Nat Acad Sci USA 104: 14249–14254
[23] Müller J, Lupton, JM, Rogach AL, Feldmann J, Talapin DV, Weller H (2004) Air induced fluorescence bursts from single semiconductor nanocrystals. Appl Phys Lett 85: 381
[24] Gomez DE, Califano M, Mulvaney P (2006) Optical properties of single semiconductor nanocrystals. Phys Chem Chem Phys 8: 4989–5011
[25] Basché T (1998) Fluorescence intensity fluctuations of single atoms, molecules and nanoparticles. J Lumin 76–77: 263–269
[26] Frantsuzov PA, Marcus RA (2005) Explanation of quantum dot blinking without the long-lived trap hypothesis. Phys Rev B 72: 155321
[27] Müller J, Lupton JM, Rogach A, Feldmann J, Talapin DV, Weller H (2005) Signatures of surface charge migration in the spectral diffusion of single elongated CdSe/CdS nanocrystals. Phys Rev B 72:205339
[28] Müller J, Lupton JM, Rogach AL, Feldmann J, Talapin DV, Weller H (2004) Monitoring surface charge movement in single elongated semiconductor nanocrystals. Phys Rev Lett 93: 167402
[29] Hohng S, Ha T (2004) Near-complete suppression of quantum dot blinking in ambient conditions. J Am Chem Soc 126: 1324–1325
[30] He H, Qian HF, Dong CQ, Wang KL, Ren JC (2006) Single nonblinking CdTe quantum dots synthesized in aqueous thiopropionic acid. Angew Chem Int Ed 45: 7588–7591
[31] Kiraz A, Ehrl M, Bräuchle C, Zumbusch A (2003) Low temperature single molecule spectroscopy using vibronic excitation and dispersed fluorescence detection. J Chem Phys 118: 10821–10824
[32] Krishnan R, Hahn MA, Yu ZH, Silcox J, Fauchet PM, Krauss TD (2004) Polarization surface-charge density of single semiconductor quantum rods. Phys Rev Lett 92: 216803
[33] Krauss TD, O'Brien S, Brus LE (2001) Charge and photoionization properties of single semiconductor nanocrystals. J Phys Chem B 105: 1725–1733
[34] Krauss TD, Brus LE (1999) Charge, polarizability, and photoionization of single semiconductor nanocrystals. Phys Rev Lett 83: 4840–4843
[35] Shim M, Guyot-Sionnest P (1999) Permanent dipole moment and charges in colloidal semiconductor quantum dots. J Chem Phys 111: 6955–6964
[36] Empedocles SA, Norris DJ, Bawendi MG (1996) Photoluminescence spectroscopy of single CdSe nanocrystallite quantum dots. Phys Rev Lett 77: 3873–3876
[37] Peng XG, Manna L, Yang WD, Wickham J, Scher E, Kadavanich A, Alivisatos AP (2000) Shape control of CdSe nanocrystals. Nature 404: 59–61
[38] Talapin DV, Koeppe R, Götzinger S, Kornowski A, Lupton JM, Rogach AL, Benson O, Feldmann J, Weller H (2003) Highly emissive colloidal CdSe/CdS heterostructures of mixed dimensionality. Nano Lett 3: 1677
[39] Alivisatos AP (1996) Semiconductor clusters, nanocrystals, and quantum Dots. Science 271: 933–937
[40] Koberling F, Mews A, Philipp G, Kolb U, Potapova I, Burghard M, Basché T (2002) Fluorescence spectroscopy and transmission electron microscopy of the same isolated semiconductor nanocrystals. Appl Phys Lett 81: 1116–1118
[41] Chung IH, Bawendi MG (2004) Relationship between single quantum-dot intermittency and fluorescence intensity decays from collections of dots. Phys Rev B 70: 165304
[42] Tang J, Marcus RA (2006) Determination of energetics and kinetics from single-particle intermittency and ensemble-averaged fluorescence intensity decay of quantum dots. J Chem Phys 125: 044703
[43] Margolin G, Barkai E (2004) Aging correlation functions for blinking nanocrystals, and other on–off stochastic processes. J Chem Phys 121: 1566–1577
[44] Tang J, Marcus RA (2005) Diffusion-controlled electron transfer processes and power-law statistics of fluorescence intermittency of nanoparticles. Phys Rev Lett 95: 107401
[45] Empedocles SA, Neuhauser R, Shimizu K, Bawendi MG (1999) Photoluminescence from single semiconductor nanostructures. Adv Mater 11: 1243–1256
[46] Gammon D, Snow ES, Shanabrook BV, Katzer DS, Park D (1996) Homogeneous linewidths in the optical spectrum of a single gallium arsenide quantum dot. Science 273: 87–90

[47] Li XQ, Wu YW, Steel D, Gammon D, Stievater TH, Katzer DS, Park D, Piermarocchi C, Sham LJ (2003) An all-optical quantum gate in a semiconductor quantum dot. Science 301: 809–811
[48] Woggon U (2007) Single semiconductor nanocrystals: physics and applications. J Appl Phys 101: 081737
[49] Leon R, Petroff PM, Leonard D, Fafard S (1995) Spatially-resolved visible luminescence of self-assembled semiconductor quantum dots. Science 267: 1966–1968
[50] Shields AJ, Stevenson RM, Thompson RM, Ward MB, Yuan Z, Kardynal BE, See P, Farrer I, Lobo C, Cooper K, Ritchie DA (2003) Self-assembled quantum dots as a source of single photons and photon pairs. Phys Stat Sol B 238: 353–359
[51] Müller J (2005) Elektrische Manipulation der Lichtemission von einzelnen CdSe/CdS Nanostäbchen. Ph.D. Thesis, University of Munich, http://edoc.ub.uni-muenchen.de/5129/
[52] Tavenner-Kruger S, Park YS, Lonergan M, Woggon U, Wang HL (2006) Zero-phonon linewidth in CdSe/ZnS core/shell nanorods. Nano Lett 6:2154–2157
[53] Le Thomas N, Allione M, Fedutik Y, Woggon U, Artemyev MV, Ustinovich EA (2006) Multiline spectra of single CdSe/ZnS core-shell nanorods. Appl Phys Lett 89: 263115
[54] Palinginis P, Tavenner S, Lonergan M, Wang HL (2003) Spectral hole burning and zero phonon linewidth in semiconductor nanocrystals. Phys Rev B 67: 201307
[55] Htoon H, Cox PJ, Klimov VI (2004) Structure of excited-state transitions of individual semiconductor nanocrystals probed by photoluminescence excitation spectroscopy. Phys Rev Lett 93: 187402
[56] Neuhauser RG, Shimizu KT, Woo WK, Empedocles SA, Bawendi MG (2000) Correlation between fluorescence intermittency and spectral diffusion in single semiconductor quantum dots. Phys Rev Lett 85: 3301–3304
[57] Empedocles SA, Bawendi MG (1999) Influence of spectral diffusion on the line shapes of single CdSe nanocrystallite quantum dots. J Phys Chem B 103: 1826–1830
[58] Koberling F, Mews A, Basché T (1999) Single-dot spectroscopy of CdS nanocrystals and CdS/HgS heterostructures. Phys Rev B 60: 1921–1927
[59] Tittel J, Gohde W, Koberling F, Basché T, Kornowski A, Weller H, Eychmuller A (1997) Fluorescence spectroscopy on single CdS nanocrystals. J Phys Chem B 101: 3013–3016
[60] Robinson HD, Goldberg BB (2000) Light-induced spectral diffusion in single self-assembled quantum dots. Phys Rev B 61: R5086–R5089
[61] Bayer M, Forchel A (2002) Temperature dependence of the exciton homogeneous linewidth in In0.60Ga0.40As/GaAs self-assembled quantum dots. Phys Rev B 65: 041308
[62] Kammerer C, Voisin C, Cassabois G, Delalande C, Roussignol P, Klopf F, Reithmaier JP, Forchel A, Gerard JM (2002) Line narrowing in single semiconductor quantum dots: toward the control of environment effects. Phys Rev B 66: 041306
[63] Moerner WE (1994) Examining nanoenvironments in solids on the scale of a single isolated impurity molecule. Science 265: 46–53
[64] Empedocles SA, Bawendi MG (1997) Quantum-confined stark effect in single CdSe nanocrystallite quantum dots. Science 278: 2114–2117
[65] Turck V, Rodt S, Stier O, Heitz R, Engelhardt R, Pohl UW, Bimberg D, Steingruber R (2000) Effect of random field fluctuations on excitonic transitions of individual CdSe quantum dots. Phys Rev B 61: 9944–9947
[66] Blome PG, Wenderoth M, Hubner M, Ulbrich RG, Porsche J, Scholz F (2000) Temperature-dependent linewidth of single InP/GaxIn1-*x*P quantum dots: interaction with surrounding charge configurations. Phys Rev B 61: 8382–8387
[67] Miller DA, Chemla DS, Damen TC, Gossard AC, Wiegmann W, Wood TH, Burrus CA (1984) Band-edge electroabsorption in quantum well structures: the quantum-confined stark effect. Phys Rev Lett 53: 2173–2176
[68] Kulik D, Htoon H, Shih CK, Li YD (2004) Photoluminescence properties of single CdS nanorods. J Appl Phys 95: 1056–1063
[69] Gomez DE, van Embden J, Mulvaney P (2006) Spectral diffusion of single semiconductor nanocrystals: the influence of the dielectric environment. Appl Phys Lett 88: 154106
[70] Klingshirn C (1998) Some selected aspects of the optical properties of II–VI semiconductor structures of reduced dimensionality. Ann Phys 23: 3–17
[71] Puzder A, Williamson AJ, Gygi F, Galli G (2004) Self-healing of CdSe nanocrystals: first-principles calculations. Phys Rev Lett 92: 217401
[72] Rothenberg E, Kazes M, Shaviv E, Banin U (2005) Electric field induced switching of the fluorescence of single semiconductor quantum rods. Nano Lett 5: 1581–1586
[73] Eychmüller A, Hässelbarth A, Katsikas L, Weller H (1991) Photochemistry of semiconductor colloids. 36. Fluorescence investigations on the nature of electron and hole traps in Q-sized colloidal CdS particles. Ber Bunsenges Phys Chem 95: 79–88

[74] Patton B, Langbein W, Woggon U (2003) Trion, biexciton, and exciton dynamics in single self-assembled CdSe quantum dots. Phys Rev B 68: 125316
[75] Warburton RJ, Schaflein C, Haft D, Bickel F, Lorke A, Karrai K, Garcia JM, Schoenfeld W, Petroff PM (2000) Optical emission from a charge-tunable quantum ring. Nature 405: 926–929
[76] Karrai K, Warburton RJ, Schulhauser C, Högele A, Urbaszek B, McGhee EJ, Govorov AO, Garcia JM, Gerardot BD, Petroff PM (2004) Hybridization of electronic states in quantum dots through photon emission. Nature 427: 135–138
[77] Klimov VI, Mikhailovsky AA, McBranch DW, Leatherdale CA, Bawendi MG (2000) Quantization of multiparticle Auger rates in semiconductor quantum dots. Science 287: 1011–1013
[78] Kraus RM, Lagoudakis PG, Müller J, Rogach AL, Lupton JM, Feldmann J, Talapin DV, Weller H (2005) Interplay between Auger and ionization processes in nanocrystal quantum dots. J Phys Chem B 109: 18214
[79] Shimizu KT, Woo WK, Fisher BR, Eisler HJ, Bawendi MG (2002) Surface-enhanced emission from single semiconductor nanocrystals. Phys Rev Lett 89: 117401
[80] Kuno M, Fromm DP, Johnson ST, Gallagher A, Nesbitt DJ (2003) Modeling distributed kinetics in isolated semiconductor quantum dots. Phys Rev B 67: 125304
[81] Zhang K, Chang HY, Fu AH, Alivisatos AP, Yang H (2006) Continuous distribution of emission states from single CdSe/ZnS quantum dots. Nano Lett 6: 843–847
[82] LeThomas N, Woggon U, Schops O, Artemyev MV, Kazes M, Banin U (2006) Cavity QED with semiconductor nanocrystals. Nano Lett 6: 557–561
[83] Biebricher A, Sauer M, Tinnefeld P (2006) Radiative and nonradiative rate fluctuations of single colloidal semiconductor nanocrystals. J Phys Chem B 110: 5174–5178
[84] Fisher BR, Eisler HJ, Stott NE, Bawendi MG (2004) Emission intensity dependence and single-exponential behavior in single colloidal quantum dot fluorescence lifetimes. J Phys Chem B 108: 143–148
[85] Brokmann X, Coolen L, Dahan M, Hermier JP (2004) Measurement of the radiative and nonradiative decay rates of single CdSe nanocrystals through a controlled modification of their spontaneous emission. Phys Rev Lett 93: 107403
[86] Labeau O, Tamarat P, Lounis B (2003) Temperature dependence of the luminescence lifetime of single CdSe/ZnS quantum dots. Phys Rev Lett 90: 257404
[87] Schlegel G, Bohnenberger J, Potapova I, Mews A (2002) Fluorescence decay time of single semiconductor nanocrystals. Phys Rev Lett 88: 137401
[88] Adams DM, Brus L, Chidsey CED, Creager S, Creutz C, Kagan CR, Kamat PV, Lieberman M, Lindsay S, Marcus RA, Metzger RM, Michel-Beyerle ME, Miller JR, Newton MD, Rolison DR, Sankey O, Schanze KS, Yardley J, Zhu XY (2003) Charge transfer on the nanoscale: current status. J Phys Chem B 107: 6668–6697
[89] Weissman MB (1988) 1/F noise and other slow, nonexponential kinetics in condensed matter. Rev Mod Phys 60: 537–571
[90] Jung SW, Fujisawa T, Hirayama Y, Jeong YH (2004) Background charge fluctuation in a GaAs quantum dot device. Appl Phys Lett 85: 768–770
[91] Hoogenboom JP, van Dijk EMHP, Hernando J, van Hulst NF, García-Parajo MF (2005) Power-law-distributed dark states are the main pathway for photobleaching of single organic molecules. Phys Rev Lett 95: 097401
[92] Schindler F, Lupton JM, Feldmann J, Scherf U (2004) A universal picture of chromophores in pi-conjugated polymers derived from single molecule spectroscopy. Proc Natl Acad Sci USA 101: 14695
[93] Schindler F, Lupton JM (2005) Single Chromophore Spectroscopy of MEH-PPV: homing-in on the elementary emissive species in conjugated polymers. Chem Phys Chem 6: 926
[94] Schindler F, Lupton JM, Müller J, Feldmann J, Scherf U (2006) How single conjugated polymer molecules respond to electric fields. Nat Mater 5: 141
[95] Schindler F, Lupton JM, Feldmann J (2006) Spontaneous switching of permanent dipoles in single conjugated polymer molecules. Chem Phys Lett: 428: 405–410
[96] Koch N (2007) Organic electronic devices and their functional interfaces. Chem Phys Chem 8: 1438–1455
[97] Arkhipov VI, Emelianova EV, Bässler H (1999) Hot exciton dissociation in a conjugated polymer. Phys Rev Lett 82: 1321–1324
[98] Falci G, D'Arrigo A, Mastellone A, Paladino E (2005) Initial decoherence in solid state qubits. Phys Rev Lett 94: 167002
[99] Yang H, Luo GB, Karnchanaphanurach P, Louie TM, Rech I, Cova S, Xun LY, Xie XS (2003) Protein conformational dynamics probed by single-molecule electron transfer. Science 302: 262–266

[100] Heller W, Bockelmann U, Abstreiter G (1998) Electric-field effects on excitons in quantum dots. Phys Rev B 57: 6270–6273
[101] Müller J, Lupton JM, Schindler F, Koeppe R, Lagoudakis PG, Rogach AL, Feldmann J, Talapin DV, Weller H (2005) Wavefunction engineering in elongated semiconductor nanocrystals with heterogeneous carrier confinement. Nano Lett 5: 2044–2050
[102] Becker K, Lupton JM, Müller J, Rogach AL, Talapin DV, Weller H, Feldmann J (2006) Electrical control of Förster energy transfer. Nat Mater 5: 777
[103] Kraus RM, Lagoudakis PG, Rogach AL, Talapin DV, Weller H, Lupton JM, Feldmann J (2007) Room-temperature exciton storage in elongated semiconductor nanocrystals. Phys Rev Lett 98: 017401
[104] Scholes GD, Jones M, Kumar S (2007) Energetics of photoinduced electron-transfer reactions decided by quantum confinement. J Phys Chem C 111: 13777–13785
[105] Michalet X, Pinaud FF, Bentolila LA, Tsay JM, Doose S, Li JJ, Sundaresan G, Wu AM, Gambhir SS, Weiss S (2005) Quantum dots for live cells, in vivo imaging, and diagnostics. Science 307: 538–544
[106] Barkai E, Jung YJ, Silbey R (2004) Theory of single-molecule spectroscopy: beyond the ensemble average. Ann Rev Phys Chem 55: 457–507
[107] Ha TJ, Ting AY, Liang J, Caldwell WB, Deniz AA, Chemla DS, Schultz PG, Weiss S (1999) Single-molecule fluorescence spectroscopy of enzyme conformational dynamics and cleavage mechanism. Proc Natl Acad Sci USA 96: 893–898.
[108] Mori T, Vale RD, Tomishige M (2007) How kinesin waits between steps. Nature 450: 750–755
[109] Deniz AA, Dahan M, Grunwell JR, Ha TJ, Faulhaber AE, Chemla DS, Weiss S, Schultz PG (1999) Single-pair fluorescence resonance energy transfer on freely diffusing molecules: observation of Förster distance dependence and subpopulations. Proc Natl Acad Sci USA 96: 3670–3675
[110] Clapp AR, Medintz IL, Mauro JM, Fisher BR, Bawendi MG, Mattoussi H (2004) Fluorescence resonance energy transfer between quantum dot donors and dye-labeled protein acceptors. J Am Chem Soc 126: 301–310
[111] Medintz IL, Uyeda HT, Goldman ER, Mattoussi H (2005) Quantum dot bioconjugates for imaging, labelling and sensing. Nat Mater 4: 435–446
[112] Willard DM, Carillo LL, Jung J, Van Orden A (2001) CdSe–ZnS Quantum dots as resonance energy transfer donors in a model protein–protein binding assay. Nano Lett 1: 469–474
[113] Kloepfer JA, Cohen N, Nadeau JL (2004) FRET between CdSe quantum dots in lipid vesicles and water- and lipid-soluble dyes. J Phys Chem B 108: 17042–17049
[114] Medintz IL, Konnert JH, Clapp AR, Stanish I, Twigg ME, Mattoussi H, Mauro JM, Deschamps JR (2004) A fluorescence resonance energy transfer-derived structure of a quantum dot-protein bioconjugate nanoassembly. Proc Natl Acad Sci USA 101: 9612–9617
[115] Zhang CY, Yeh HC, Kuroki MT, Wang TH (2005) Single-quantum-dot-based DNA nanosensor. Nat Mater 4: 826–831
[116] Soujon D, Becker K, Rogach AL, Feldmann J, Weller H, Talapin DV, Lupton JM (2007) Time resolved Förster energy transfer from individual semiconductor nanoantennae to single dye molecules. J Phys Chem C 111: 11511
[117] Potapova I, Mruk R, Hübner C, Zentel R, Basché T, Mews A (2005) CdSe/ZnS nanocrystals with dye-functionalized polymer ligands containing many anchor groups. Angew Chem Int Ed 44: 2437–2440
[118] Barth M, Schuster R, Gruber A, Cichos F (2006) Imaging single quantum dots in three-dimensional photonic crystals. Phys Rev Lett 96: 243902
[119] Gudiksen MS, Maher KN, Ouyang L, Park H (2005) Electroluminescence from a single-nanocrystal transistor. Nano Lett 5: 2257–2261
[120] Huang H, Dorn A, Bulovic V, Bawendi MG (2007) Electrically driven light emission from single colloidal quantum dots at room temperature. Appl Phys Lett 90: 023110
[121] Huynh WU, Dittmer JJ, Alivisatos AP (2002) Hybrid nanorod-polymer solar cells. Science 295: 2425–2427
[122] Hettich C, Schmitt C, Zitzmann J, Kuhn S, Gerhardt I, Sandoghdar V (2002) Nanometer resolution and coherent optical dipole coupling of two individual molecules. Science 298: 385–389.
[123] Ortner G, Bayer M, Lyanda-Geller Y, Reinecke TL, Kress A, Reithmaier JP, Forchel A (2005) Control of vertically coupled InGaAs/GaAs quantum dots with electric fields. Phys Rev Lett 94: 157401
[124] Krenner HJ, Sabathil M, Clark EC, Kress A, Schuh D, Bichler M, Abstreiter G, Finley JJ (2005) Direct observation of controlled coupling in an individual quantum dot molecule. Phys Rev Lett 94: 057402
[125] Fernee MJ, Rubinsztein-Dunlop H (2006) Quantum gate based on Stark tunable nanocrystal interactions with ultrahigh-Q/V field modes in fused silica microcavities. Phys Rev B 74: 115321